JOURNAL OF GEOPHYSICAL RESEARCH, VOL. 99, NO. B12, PAGES 24,275–24,300, DECEMBER 10, 1994

Fluid dynamic and geochemical aspects of entrainment in mantle plumes

Erik H. Hauri,[1] John A. Whitehead, and Stanley R. Hart

Woods Hole Oceanographic Institution, Woods Hole, Massachusetts

Abstract. A similarity solution has been developed for vertical, steady-state mantle plume conduits by considering the boundary layer flow emanating from a point source of heat in an axisymmetric geometry. This model includes the effects of temperature and shear stress on viscosity, and incorporates depth-dependent viscosity and thermal expansivity. Plumes with variable viscosity have upward velocities of 0.30-100 m/yr and radii of 30-250 km, depending on temperature, rheology and buoyancy flux. These results demonstrate the small lateral scale of plume features relative to the resolution of most large-scale convection models and seismological studies. All of the plumes studied showed significant entrainment of ambient mantle surrounding the plume conduit, driven by the radial conduction of heat from the plume. This heat raises the buoyancy and lowers the viscosity of the ambient mantle, thereby entraining it into the conduit flow. For buoyancy fluxes of 0.1-10 Mg/s, similar to the range estimated for plumes in the Earth's mantle, we calculate a range of entrainment of >90% to <5% ambient mantle, correlating negatively with buoyancy flux. Examination of the streamlines of mantle material which is entrained into thermal plumes indicates that most of the entrained fraction originates from approximately the lower half of the layer traversed by the plume, and shows minor entrainment of upper level material. This is especially true for non-Newtonian and depth dependent rheologies, and for depth-dependent thermal expansivity. Upwelling of depleted upper mantle, viscously coupled to the plume flow, is proposed as a mechanism for generating post-shield stage alkalic basalts erupted on oceanic island chains and their associated flexural arches. The existing Sr-Nd-Pb isotope data for oceanic basalts indicate the presence of a component which is common to hotspot basalts worldwide, and which is distinct from the upper mantle source of mid-ocean ridge basalts. This component (termed "FOZO" by Hart et al. (1992)) has moderately depleted Sr and Nd signatures, radiogenic Pb isotopes, and elevated $^3He/^4He$ ratios. The high He isotope ratios of FOZO suggest an origin for this component in the lower mantle, and would appear to provide independent evidence to support the fluid dynamic observations for significant entrainment of lower mantle in plumes and exclusion of upper mantle. If the composition of FOZO is representative of the isotopic composition of the lower mantle, then it would appear that this reservoir has been differentiated relative to estimates for the bulk silicate earth (BSE). This may be due either to melting and differentiation at higher levels in the mantle, or to fractionation of high pressure phases from a terrestrial magma ocean.

Introduction

The chemical heterogeneity of the Earth has been unequivocally demonstrated through geochemical investigations of the crust and mantle. These chemical variations reflect the relative efficiency of those processes which attempt to homogenize the Earth. The scale at which solid-phase diffusion is capable of erasing geochemical variability is limited to meters, even at lower mantle temperatures over the age of the Earth [*Hofmann and Hart*, 1978]. Thus advection of mass must be the most important mechanism by which the scale and magnitude of geochemical variability are modulated [*Richter and Ribe*, 1979; *Olson et al.*, 1984]. It is now well accepted that the Earth's mantle behaves as a viscous fluid over geologic timescales [*Turcotte and Oxburgh*, 1969; *Goetze and Kohlstedt*, 1973], and thus the scale, variance and amplitude of isotopic heterogeneity present in the convecting mantle must reflect the mixing efficiency of various convective processes operating in the interior of the Earth [*Allegre*, 1987]. Since shear strain mixing is probably the dominant mixing mechanism in the deep mantle, the importance of variations in mantle viscosity in preserving or destroying heterogeneity cannot be overestimated. For example, to first order, the spatial scale and amplitude of isotopic heterogeneity in the continental crust are largely the result of a much slower mixing timescale due to a much higher effective viscosity compared with the mantle. In this respect, the likelihood of a heterogeneous distribution of shear in the mantle suggests that heterogeneities can be preserved for billions of years in the presence of convection [*Davies*, 1984]. Thus, the effects of parameters which determine the viscosity of the mantle (pressure, temperature, shear stress, melt fraction, composi-

[1]Now at Department of Terrestrial Magnetism, Carnegie Institution of Washington, Washington, D.C.

Paper number 94JB01257.
0148-0227/94/94JB-01257$05.00

tion, phase stability, etc.) must be incorporated into any model of mantle convection which attempts to evaluate the ability of a viscous fluid to maintain or destroy compositional variability.

The heterogeneous nature of the convecting mantle has been largely delineated through the geochemical study of mid-ocean ridge basalts (MORB) and oceanic island basalts (OIB) [e.g., *Zindler and Hart*, 1986; *Allegre et al.*, 1987]. Although there is significant heterogeneity within MORB from various ocean basins [e.g., *Allegre et al.*, 1984; *Ito et al.*, 1987], the total isotopic variability exhibited by normal-type MORB is substantially less than that in OIB [*Hart*, 1988], and this must be a reflection of different convective regimes in the sources of these mantle-derived magmas. The source of MORB is the uppermost mantle, and it is well accepted that MORB is generated by passive upwelling due to lithospheric extension beneath the ridges [e.g., *McKenzie and Bickle*, 1988]. It is also generally well accepted that many (though possibly not all) OIB are generated by relatively fixed, upwelling plumes in the mantle beneath a moving lithosphere, the hotspot hypothesis of *Wilson* [1963] and *Morgan* [1972]. Such plumes are a robust feature of any fluid mechanical description of the Earth, and provide a compelling mechanism for the creation of age-progressive linear island chains [e.g., *Duncan and McDougall*, 1976]. Since most OIB are the products of melting in mantle plumes, the study of buoyant plumes in viscous fluids should provide constraints on how the signal of isotopic variability in the mantle is transferred to magmas erupted at oceanic islands.

In this paper, we assume that a heterogeneous mantle source is delivered to the base of the oceanic lithosphere by buoyant mantle plumes, and that this mantle heterogeneity is the result of mixing of at least two distinct mantle components down to the length scale of sampling by the melting process (≤25 km [*Frey and Rhodes*, 1993]). This mixture of components can develop in essentially two ways. In the first, which we will call convective mixing, two or more distinct components in the earth's interior, which may be indigenous or introduced through subduction, are juxtaposed and mixed by large-scale convective processes, with the mixed package delivered to the surface in a mantle plume. In the second process, which we refer to as entrainment, distinct components may be juxtaposed and mixed during the actual dynamical processes associated with the plume flow itself. *Griffiths* [1986] examined the entrainment of ambient mantle into individual spherical diapirs. *Sleep* [1988] examined the entrainment of a dense layer at D" into the central region of a mantle upwelling, which we refer to as cusp entrainment. *Griffiths and Campbell* [1991] studied the entrainment of ambient mantle by inclined plumes in the presence of a background convective flow. Despite the advances made by these studies, the simplest case of entrainment of surrounding, ambient mantle by steady state, vertical plumes has not been examined, and few attempts have been made to examine hotspot geochemistry in the fluid dynamic context of mantle plumes undergoing entrainment.

It is with this strategy that we have developed a similarity solution of a boundary layer model for examination of the flow in vertical, steady state mantle plume conduits. It is likely that hot, buoyant plumes in the mantle transfer some of their thermal signature to the surrounding ambient mantle, thus increasing the buoyancy and lowering the viscosity of this material. In this way, the ambient mantle surrounding the plume may be entrained into the flow [*Griffiths*, 1986; *Richards and Griffiths*, 1989]. As a result, depending on the details of the flow inside plume conduits, the plume material which is delivered to the base of the lithosphere is potentially a mixture of all levels of mantle through which the plume has passed on its way to the lithosphere. In this way, mantle plumes may act as "sampling probes" by entraining mantle from various depths between their source regions and the lithosphere. Viscosity variations should play a role of substantial importance in entrainment, and so we have explicitly included the effects of temperature and shear stress on viscosity, which allows the incorporation of experimentally constrained rheologies, such as for olivine [*Goetze and Kohlstedt*, 1973; *Kohlstedt et al.*, 1976]. In addition, variations in thermal diffusivity, and the dependence of thermal expansivity and viscosity with depth are examined. All of these effects have significant influence on the nature of flow and entrainment in mantle plume conduits.

Numerical Results

As an analog for a mantle plume conduit (ignoring the ultimate source of the conduit and interaction with the lithosphere), this study examines the axisymmetric upwelling above a point source of heat in an infinite volume of fluid (Figure 1). In addition to the velocity, temperature, viscosity and shear stress structure of mantle plume conduits, we wish to examine the entrainment of ambient mantle (that part of the mantle which surrounds the plume), study how this entrainment is effected by plume flux, mantle rheology, and

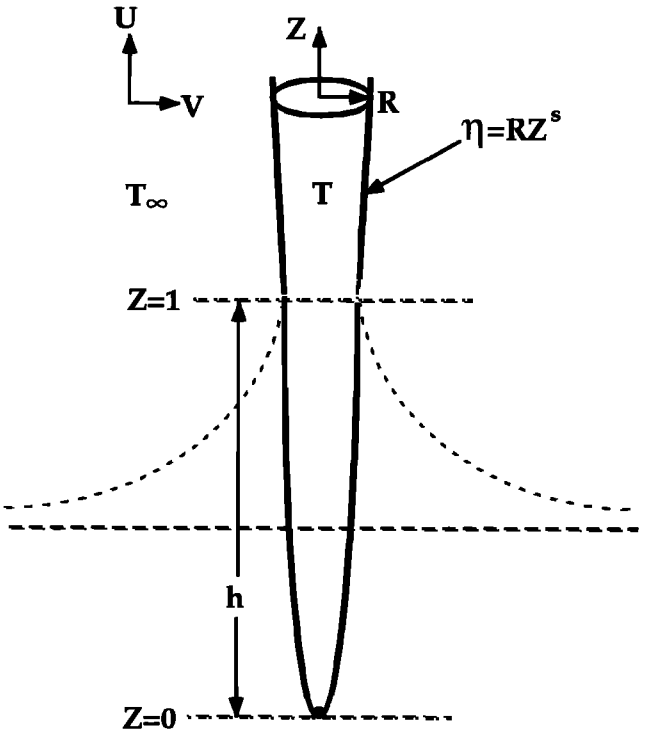

Figure 1. Geometry of the axisymmetric boundary layer emanating from a point source of heat (solid line). The point source (Z=0, dashed line) is assumed to lie a distance h below the base of the plume conduit (Z=1, dashed line). The model only describes the plume conduit; the cusp which attaches the conduit to a horizontal boundary layer (dotted lines) is not modeled.

Table 1. Physical Properties and Constants

Symbol	Definition	Values
R,Z	radial, height coordinates	-----
h	characteristic scale length	variable
U,V	vertical, horizontal velocities	-----
T	temperature	-----
T_0	ambient temperature	1300 °C
ΔT_{base}	axial ΔT at base of plume	variable
ΔT_{top}	axial ΔT at top of plume	100-400 °C
α	coefficient of thermal expansion	3×10^{-5} $°C^{-1}$
κ	thermal diffusivity	2.5×10^{-6} $m^2 s^{-1}$
τ	shear stress	-----
μ	viscosity	-----
Q_V	volume flux	-----
Q_m	mass flux	-----
Q_B	buoyancy flux	-----
D	depth of layer, length of conduit	-----
M_1	pre-exponential factor (n=1)	1 $kg\ m^{-1}\ s^{-1}$
M_2	pre-exponential factor (n=3)	3.25×10^{-10} $kg^3\ m^{-3}\ s^{-5}$
C_1, a	depth-dependent α constants*	-----
C_2, b	depth-dependent M constants†	-----
E	viscous creep activation energies	0-523 $kJ\ mol^{-1}$
n	power law exponent	1,3
A,B	rheological parameters	fit to activation energies

* Adjusted for a factor of 6 decrease in α through 2700 km depth.

† Adjusted for a factor of 100 increase in μ through 2700 km depth.

depth-dependent properties, and ultimately constrain the origin of the mantle which is entrained into these vertical plumes. The point-source boundary layer equations of *Schlichting* [1968] were modified to account for temperature-, stress-, and depth-dependent viscosity, as well as depth-dependent thermal expansivity. The equations were solved by the use of a similarity solution which resembles the point-source axisymmetric solutions of *Brand and Lahey* [1967] and *Liu and Chase* [1991]. The present analysis differs primarily in our explicit modeling of variable viscosity and thermal expansivity. Our analysis is most similar to the variable-viscosity model of *Yuen and Schubert* [1976], who examined the boundary layer created next to a planar source of heat. Although we assume a steady state and self-similarity, this type of analysis has the advantages of numerical simplicity while fully retaining all the nonlinearities of the problem. In addition, it is computationally economical to use a very fine grid spacing, so that features within individual plumes with large changes in viscosity are resolved, and accurate calculations of the amounts of entrainment are easily made. The derivation of the solution for this problem is given in the appendix, and definitions and values of various parameters are given in Tables 1 and 2.

Table 2. Fits of Eq. (A6) to Arrhenius Functions With Variable Activation Energies

ActivationEnergy, kJ/mol	A	B
523	0.30428	1.37×10^{-4}
423	0.26190	1.50×10^{-4}
323	0.20130	1.72×10^{-4}
223	0.10213	2.17×10^{-4}
0	0	0

Newtonian Rheologies

Radial profiles of ΔT, vertical velocity, and shear stress for the Newtonian (n=1) constant viscosity ($\mu=10^{21}$ Pa s) case are shown in Figure 2. For each rheology, the vertical velocity on the axis of the plume increases with increasing ΔT. Figure 3 shows some of the same results for a Newtonian rheology with a temperature dependent viscosity (523 kJ/mol activation energy). It is apparent that the vertical velocities are much higher for the case where viscosity decreases with increasing temperature. These plumes show a decrease in viscosity as temperature increases toward the center of the plume (Figure 3c). For a fluid with a temperature dependent viscosity, heat plays the dual role of providing buoyancy and lowering viscosity, both of which promote the upward movement of fluid.

Qualitatively, the relationship between plume radii and viscosity is reflected in the equation for flow in a pipe:

$$r = \left(\frac{8 Q_m \mu}{\pi g\ \Delta\rho} \right)^{1/4} \tag{1}$$

where Q_m is the plume mass flux. At constant Q_m, the plume radius increases with increasing viscosity. In the present case, plume viscosity is largely determined by temperature (n=1 rheologies) or the combined effects of temperature and shear stress (n>1 rheologies, (A4) and (A6)). Thus, with Q_m and $\Delta\rho$ held constant, plumes with temperature-dependent rheologies are narrower than constant-viscosity plumes, and plumes with peridotite rheologies (n>1) are narrower still.

For the purposes of comparing different plumes with different rheologies, excess temperatures, and so on, it is convenient to use the plume buoyancy flux as a measure of

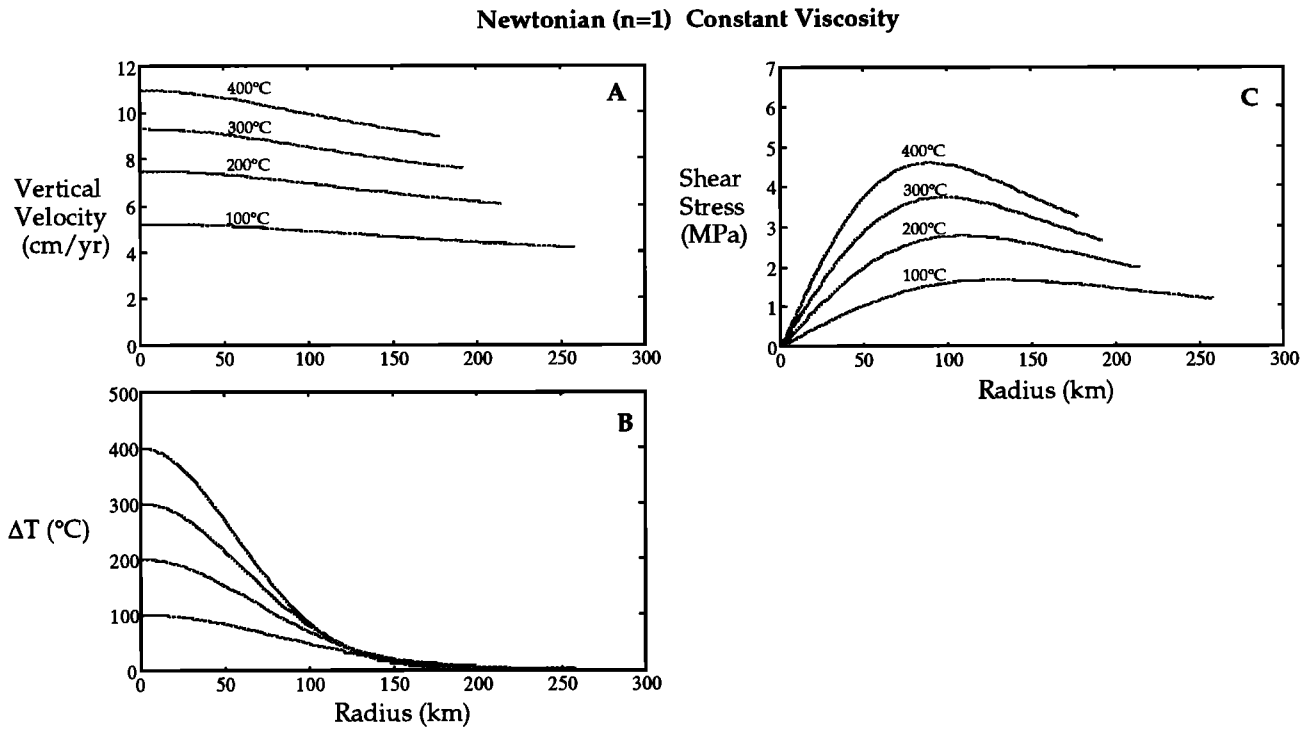

Figure 2. (a) Vertical velocity, (b) excess temperature, and (c) shear stress as a function of radius for n=1, 0 kJ/mol rheology. In this and subsequent similar figures, these results are calculated at a height of 2700 km above the base of the plume. The four curves represent plumes with values of the ratio $\Delta T_{base}/\Delta T_{top}$=2 (50% entrainment) and values of ΔT_{top}=100, 200°, 300°, and 400°C. Velocity and shear stress curves are shown out to the radius of the plume boundary, defined where the excess temperature decreases to 1% of the temperature excess on the plume axis. The velocity profiles are very flat, due to a high, constant viscosity (10^{21} Pa s).

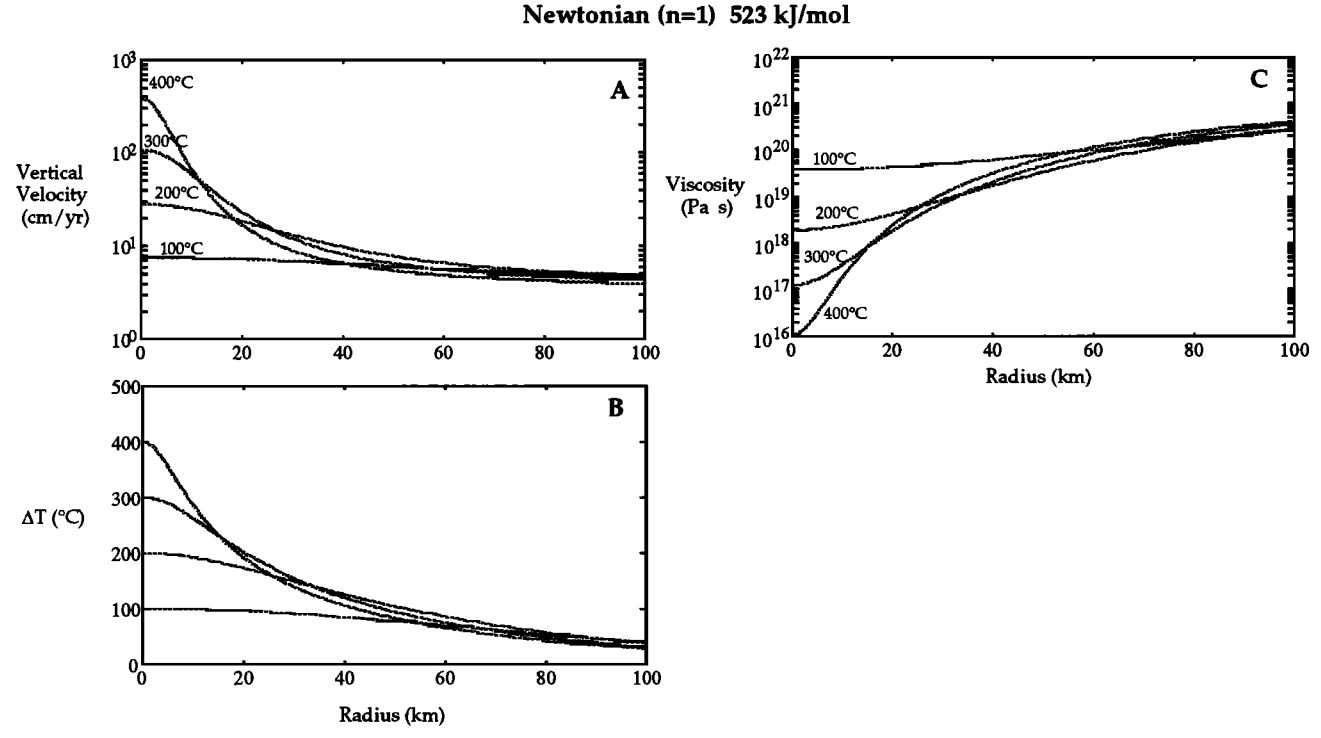

Figure 3. (a) Vertical velocity, (b) excess temperature, and (c) viscosity as a function of radius for n=1, 523 kJ/mol rheology. Due to the effect of temperature-dependent viscosity, the velocity and profiles show a concentration of high velocities around the axis of the plume, reflecting the high temperatures of this region. Plume radii, defined as 1% of axial ΔT, are off scale to right at 175-300 km.

plume strength. The definition of buoyancy flux used here is the same as used by *Sleep* [1990]:

$$Q_B = Q_m \alpha \overline{\Delta T} \quad (2)$$

where Q_m is the plume mass flux, α is the coefficient of thermal expansion, and $\overline{\Delta T}$ is the excess temperature integrated over the cross-sectional area of the plume conduit. The relationships between buoyancy flux and axial vertical velocity, plume radius, and entrainment are shown in Figure 4 (constant viscosity) and Figure 5 (temperature-dependent viscosity similar to olivine). Constant viscosity plumes with lower buoyancy fluxes will lose a larger fraction of their initial excess temperatures. Axial velocity and plume radius increase with increasing buoyancy flux for the Newtonian constant viscosity case. Lowering the overall viscosity by a factor of 100 gives the results shown in Figure 6 (compare with Figure 5). At a given buoyancy flux and ΔT_{top}, when the overall fluid viscosity is decreased by two orders of magnitude, plume radii are about 3 times smaller ($100^{1/4}$), and velocities are about 10 times higher ($u \sim r^2/\mu$) as suggested by (1). However, the influence of ambient viscosity on entrainment is negligible; the entrainment-buoyancy flux curves are virtually identical in Figure 6c.

Axial velocities for the constant viscosity plumes range from 3 to 30 cm/yr, similar to plate velocities [*Duncan and McDougall*, 1976] and plume radii range from 150 to 400 km, considerably larger than thicknesses predicted for oceanic

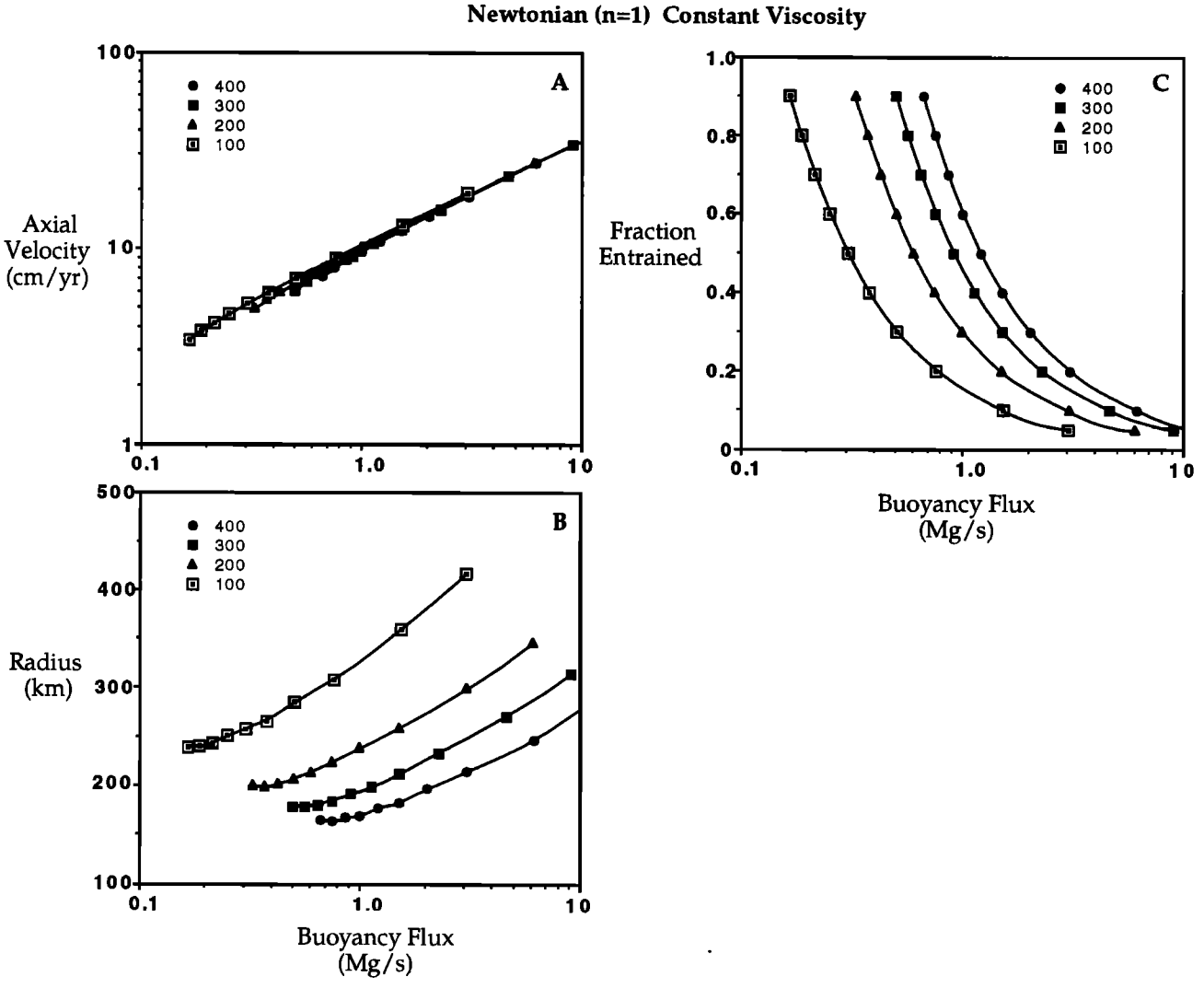

Figure 4. (a) Axial vertical velocity, (b) plume radius, and (c) amount of entrainment versus buoyancy flux for a Newtonian, constant viscosity rheology (profiles shown in Figure 2). In these figures and similar figures to follow, the parameters displayed were calculated at a height of 2700 km above the base of the plumes. Each panel shows curves for values of ΔT_{top} (100°C open square with dot, 200°C solid triangle, 300°C solidsquare, and 400°C solid circle), where ΔT_{top} is the axial excess temperature at a height of 2700 km. Each curve has symbols corresponding to various ratios of $\Delta T_{base}/\Delta T_{top}$ of 10, 3.33, 2.5, 2.0, 1.67, 1.43, 1.25, 1.11, and 1.05, in order of increasing buoyancy flux (ΔT_{base} is the axial excess temperature at the base of the plume). Plumes with higher buoyancy fluxes experience less cooling ($\Delta T_{base}/\Delta T_{top}$ closer to 1) across the depth of the fluid layer. Plumes with higher temperatures at a given buoyancy flux show more entrainment of ambient mantle.

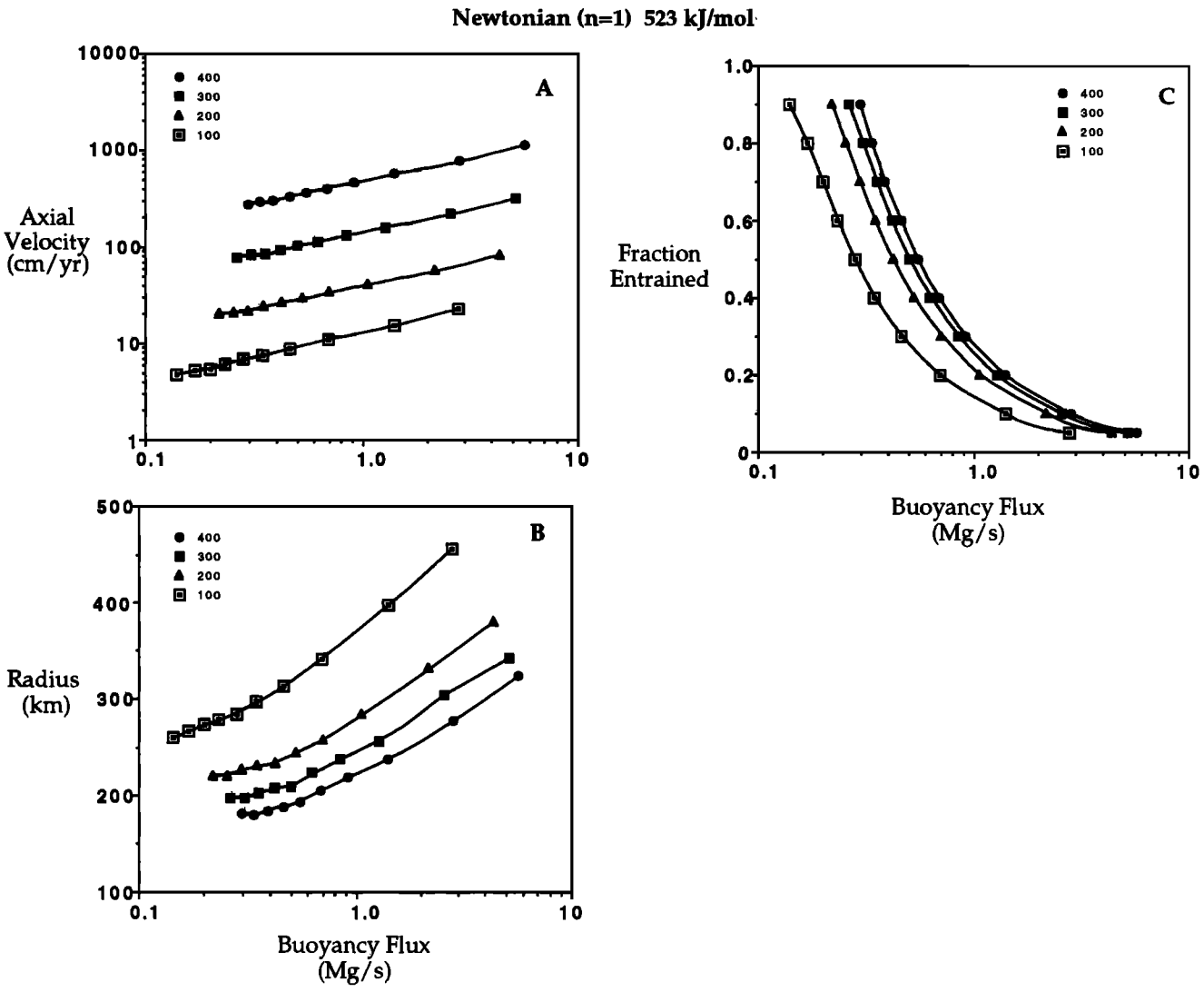

Figure 5. (a) Axial vertical velocity, (b) plume radius, and (c) amount of entrainment versus buoyancy flux for n=1, 523 kJ/mol rheology (profiles shown in Figure 3). This temperature-dependent rheology concentrates flow along the axis of the plume, resulting in higher vertical velocities compared to the constant viscosity case. However, heat is still conducted into the ambient mantle, such that plume radii in these cases are only marginally smaller than for the constant viscosity rheology (Figure 4).

lithosphere [*Parsons and Sclater*, 1977]. Our constant viscosity results can be compared with other numerical studies of constant viscosity plumes. *Watson and McKenzie* [1991] describe an axisymmetric plume which matches geoid, topography and melt production observations for the Hawaiian swell. This plume has an excess temperature of 278°C, a radius of approximately 200 km, a viscosity of 3.1×10^{19} Pa s, and a buoyancy flux of 1.4 Mg/s. *Liu and Chase* [1991] also describe constant-viscosity plumes (2×10^{18} to 2×10^{19} Pa s) which are consistent with the models of *Liu and Chase* [1989] for the Hawaiian swell. These plumes have excess temperatures of 200 to 300°C, radii of 30 to 60 km, and buoyancy fluxes around 3.1 Mg/s. Using these reported values of temperature, radius and viscosity as constraints, our model calculates plumes with axial upward velocities which are generally within 15% of the velocities calculated by *Watson and McKenzie* [1991] (0.30 m/yr) and *Liu and Chase* [1991] (0.5 to 1.7 m/yr). The smaller radii of the *Liu and Chase* [1991] plumes compared with the *Watson and McKenzie* [1991] plume can be attributed to lower bulk viscosity and higher buoyancy flux for the former.

Many large-scale convective studies have utilized variable viscosity, however these studies lack sufficient resolution to examine individual plume structures in detail, making comparisons difficult. Three studies dealing with smaller-scale problems provide some basis for comparison with our temperature-dependent viscosity results. *Yuen and Schubert* [1976], using an approach similar to the present study, examined two-dimensional plumes with variable viscosity which show qualitative agreement with the present analysis. Coupled with a thermal boundary layer analysis, *Loper and Stacey* [1983] described a variable-viscosity plume with an excess temperature of 700°C, radius of 8 km, upward velocity of 4.8 m/yr, and a buoyancy flux of 2 Mg/s. For this buoyancy flux, our model predicts an upward velocity of about 5 m/yr for an excess temperature of only 380°C (Figure 5), and a radius of 250 km. These differences are mainly due to two things. First is our use of a stronger temperature dependence

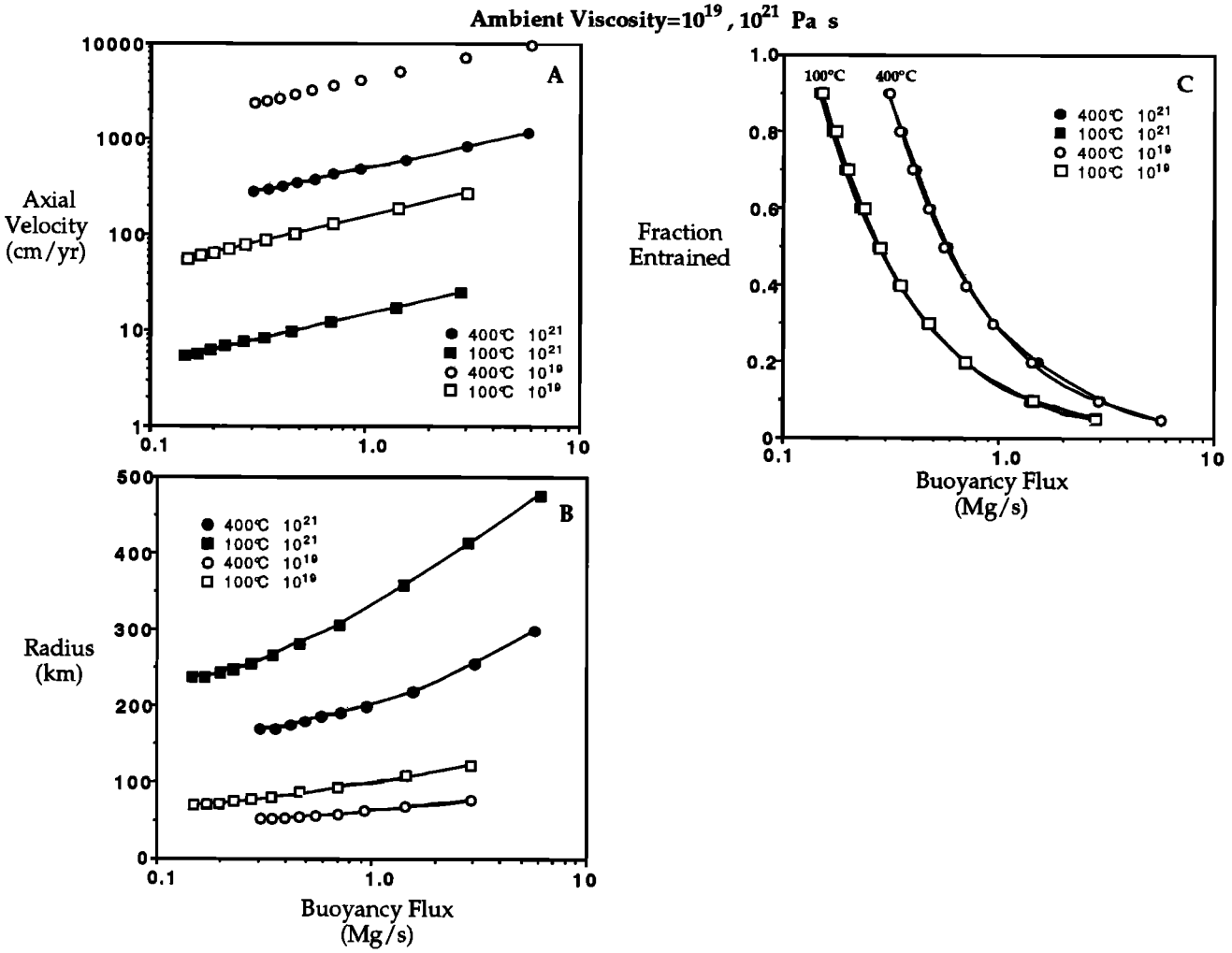

Figure 6. (a) Axial vertical velocity, (b) plume radius, and (c) amount of entrainment versus buoyancy flux for plumes with n=1, 523 kJ/mol rheology with ΔT_{top}=100°C (squares) and 400°C (circles), comparing the effects of differences in ambient viscosity (10^{19} Pa s open symbols, 10^{21} Pa s solid symbols). A factor of 100 lower ambient viscosity results in higher velocities and smaller plume radii, but entrainment-buoyancy flux relationships at the top of the plume are unchanged.

for the viscosity, resulting in a viscosity which is lower by a factor of 10 than that used by *Loper and Stacey* [1983]. Second, *Loper and Stacey* [1983] only considered the central part of the plume where velocities and temperatures are highest, well within the plume's thermal halo, whereas we have defined our plume boundary at the edge of the thermal halo. However, our observations indicate that, for strongly temperature-dependent fluids, thermal plumes consist essentially of a narrow, high-velocity boundary layer within a somewhat larger thermal halo, in agreement with the analysis of *Loper and Stacey* [1983]. *Ribe and Christensen* [1994] describe a plume which reproduces the topographic characteristics of the Hawaiian swell, using a temperature-dependent viscosity about half as strong as olivine. This plume has an excess temperature of 300°C, radius of 92 km, and a buoyancy flux of 4 Mg/s, with velocities on the order of several meters per year. Our calculations using the same parameters are in good agreement.

Entrainment of Ambient Mantle

Fractional entrainment refers to the fraction of the total mass flux at the top of the plume (2700 km height) which is due to ambient material. For all the plumes studied, the mass flux at the top of the plume is larger than at the base of the plume; this excess is due to the entrainment of ambient mantle through the sides of the plume conduits. In Figures 4 and 5, entrainment is shown to decrease with increasing buoyancy flux; this is a general feature of plume entrainment which does not depend on the physical properties of the fluid. The ambient mantle is entrained due to the conduction of heat in the radial direction; this heat increases the buoyancy of the ambient mantle and lowers its viscosity, thus incorporating this material into the plume flow. This entrainment is illustrated in Figure 7, which shows the streamlines (light lines) and plume boundary (heavy line) for a Newtonian, temperature-dependent plume with a buoyancy flux of 0.6 Mg/s and ΔT_{top}=400°C. The streamlines are observed to cross the boundary of the plume, and this plume boundary increases with height due to the entrainment of ambient mantle. The dotted streamline, which originates at the plume edge near the base of the plume, marks the boundary between the plume source mantle in the center, and the entrained ambient mantle at the periphery of the plume. The entrained fraction is further divided into material which originates from the lower mantle

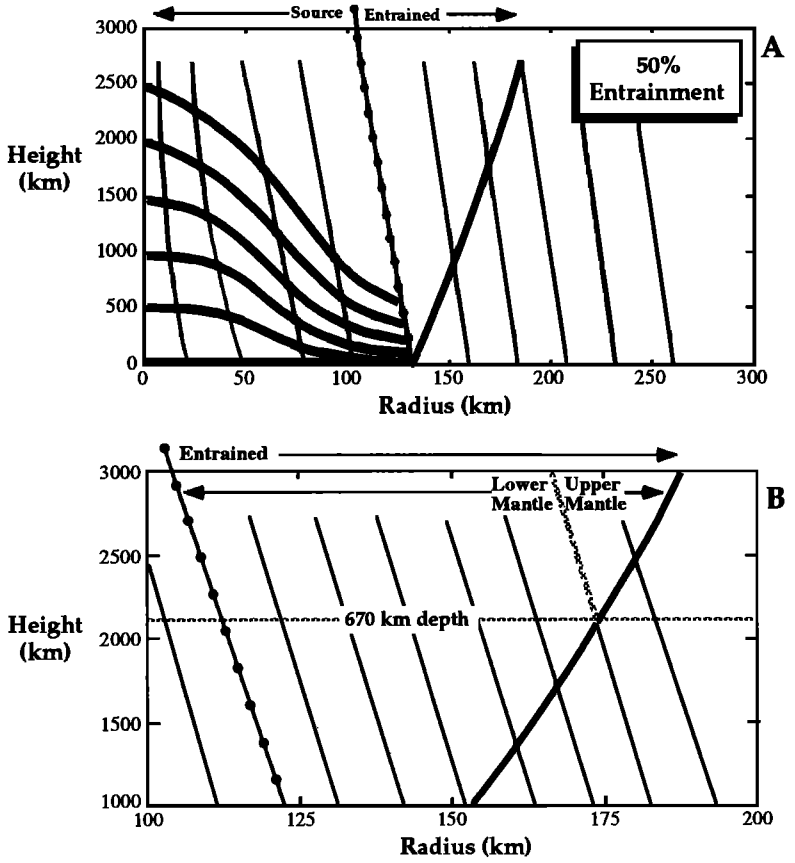

Figure 7. Flow field calculated for a plume with n=1, 523 kJ/mol rheology, with ΔT_{base}=800°C and ΔT_{top}=400°C. Streamlines are shown as light lines, and the plume boundary is shown by the single heavy line, showing an increase in radius with height (s= -1/2). (a) Entrainment is shown by streamlines which cross the plume boundary. The dotted streamline represents the boundary between plume source mantle and entrained ambient mantle. The series of heavy lines near the plume axis represent the time evolution of a 50 km thick layer of plume source material which enters the bottom of the conduit. With time, the layer, originally 125 km long, is strongly deformed and stretched to over 20 times its original length (note horizontal exaggeration). This indicates that significant shearing and deformation of different parcels of mantle occur during flow in the conduit. (b) Expanded view of the upper 1700 km of the entrained part of the plume. By tracking streamlines back into the ambient mantle outside the plume boundary, we see that the entrained mantle consists of lower mantle material (between dotted and gray streamlines) and upper mantle material (between gray streamline and plume boundary) entrained above the 670 km discontinuity.

(depths >670 km) and the upper mantle (depths <670 km, Figure 7b). This can be found by tracing the streamlines back to their intersection with the plume boundary. Thus, in the case of a laminar, vertical, steady state plume conduit, entrained mantle takes the form of radially concentric regions surrounding a core of plume source material.

In addition, significant shearing and redistribution of plume material occurs within the plume conduit. Figure 7a shows the evolution of a layer, 50 km thick, of plume source material which enters the bottom of the conduit. The layer, originally 125 km long, is sheared and stretched to about 20 times its original length within the conduit, due to the differential velocities along different streamlines. Material which starts at the plume boundary (R=125 km) is progressively pushed closer to the axis due to the slow radial inflow of entrained mantle, indicating that the plume source material is effectively redistributed toward the plume axis. Although this laminar entrainment process does not result in intimate mixing of the plume and ambient components on a small scale, as in turbulent mixing, significant juxtaposition and translation of different parcels of mantle does occur during flow in plume conduits.

The calculated buoyancy fluxes of the plumes in this study range from 0.1 to 10 Mg/s, similar to the range estimated for plumes in the Earth's mantle based on swell models [*Davies*, 1988; *Sleep*, 1990; *Ribe and Christensen*, 1994]. For this range of buoyancy fluxes, entrainment varies from >90% to <5%. Entrainment decreases with increasing buoyancy flux in general, but increases with ΔT_{top} at a given buoyancy flux. Relative to the constant viscosity case, the effect of a temperature-dependent viscosity is to decrease the amount of entrainment for a given buoyancy flux and ΔT_{top}.

The relationship between entrainment and excess temperature for individual plumes can be derived directly from the definition of the stream function. The plume boundary is defined as the value of η where θ decreases to <1% of the axial value; call this value η_t. In this two-dimensional axisymmetric geometry, streamlines bound regions of constant

mass flux. As a result, the ratio of the mass flux at any height D to the mass flux at the base of the plume is given by

$$\frac{\Psi(\eta_t,\ D\ \text{km})}{\Psi(\eta_t,\ 0\ \text{km})}=\frac{\left(\frac{D+h}{h}\right)f(\eta_t)}{\left(\frac{0+h}{h}\right)f(\eta_t)}=\frac{\Delta T_{\text{base}}}{\Delta T_{\text{top}}} \tag{3}$$

where the definition of the stream function is (A18), equation (A33) was used for dimensionless height z, and (A34) was used for the relationship between D, h, and the excess temperatures. From this relationship, we can define fractional entrainment as the fraction of the plume mass flux at the top of the plume which consists of entrained mantle:

$$\text{Entrainment}=\left[1-\frac{\Psi(\eta t,\ 0\ \text{km})}{\Psi(\eta_t,\ 2700\text{km})}\right]=\left[1-\frac{\Delta T_{\text{top}}}{\Delta T_{\text{base}}}\right] \tag{4}$$

Thus, the amount of entrainment is directly related to the drop in the plume's axial temperature across its length. Since plume buoyancy flux is constant along the length of the plume (for constant α), this same relationship can be derived from the expressions for buoyancy flux at the base and top of the plume (2).

The effects of various parameters on entrainment can be qualitatively estimated using the equations for constant viscosity laminar flow in a pipe. With a conduit of radius r and length L, the volume flux at the bottom of the conduit is

$$Q_v(r)=\frac{\pi g\ \Delta\rho\ r^4}{8\upsilon} \tag{5}$$

where υ is the kinematic viscosity. The time it takes for fluid to travel from the bottom to the top of the conduit of length L is

$$t_t=\frac{L}{U} \tag{6}$$

where U is the vertical velocity. In the time interval t_t, the sides of the conduit will have conducted heat laterally into the mantle a distance

$$\Delta r=\sqrt{\kappa t_t}=\sqrt{\frac{\kappa L}{U}}\ . \tag{7}$$

Because of the increase in radius, the volume flux at the top of the conduit is now

$$Q_v(r+\Delta r)=\frac{\pi g\ \Delta\rho\left(r+\sqrt{\frac{\kappa L}{U}}\right)^4}{8\upsilon}\ . \tag{8}$$

Material is still flowing into the bottom of the conduit with volume flux $Q_V(r)$, so more mantle is flowing out the top than is flowing in the bottom due to entrainment. The ratio of the top flux to the bottom flux (R_Q) is

$$R_Q=\frac{Q_v(r+\Delta r)}{Q_v(r)}=\frac{\left(r+\sqrt{\frac{\kappa L}{U}}\right)^4}{r^4}=\left(1+\sqrt{\frac{\pi\kappa L}{Q_v}}\right)^4\approx\frac{\Delta T_{\text{base}}}{\Delta T_{\text{top}}} \tag{9}$$

where the relationship $U=Q_V/\pi r^2$ was used, and the relationship with the ratio $\Delta T_{\text{base}}/\Delta T_{\text{top}}$ is from (3). Entrainment increases with R_Q. Thus from (9) we can see approximately that entrainment will correlate negatively with plume flux (Q_V), as shown by Figures 4 and 5. In addition, plume length (L) and thermal diffusivity (κ) will have positive effects on entrainment.

Non-Newtonian Rheologies

Non-Newtonian rheologies are characterized by the dependence of viscosity on shear stress, and values of $n>1$ indicate that viscosity decreases with increasing shear stress. In this paper, only cases with $n=3$ have been considered, though any value may be incorporated into the model. Figure 8 displays radial profiles for several plumes with a non-Newtonian rheology which has no temperature dependence; thus viscosity is a function of shear stress only. The viscosity distribution in Figure 8c is characterized by an extremely high viscosity at the plume axis, where shear stresses are low, and a sharp decrease to a viscosity minimum which corresponds to a maximum in the shear stress distribution (Figure 8d). Viscosity is still low outside the thermal boundary layer due to a substantial shear stress in the far field. Plume axial velocities correlate positively with excess temperature, but the velocity distribution is very shallow out to a distance of 20 to 30 km from the plume axis, then drops sharply away from this high velocity plateau. This "plug flow" is due to the very high viscosity of the material at the center of the plume, which is due to the inverse dependence of viscosity on shear stress, making this material stiff and difficult to deform. A similar broadening of the axial flow in non-Newtonian plumes was found by *Loper* [1984]. This type of "plug flow" is characteristic of non-Newtonian rheologies with $n>1$.

Figure 9 shows radial profiles for plumes with $n=3$ and an activation energy of 523 kJ/mol, a rheology which is similar to that determined experimentally for olivine by *Goetze and Kohlstedt* [1973] and *Kohlstedt et al.* [1976]. For the same excess temperature, vertical velocities are about an order of magnitude higher than the purely stress-dependent rheology in Figure 8, and the radial profiles of velocity, temperature, and viscosity are correspondingly smaller. Figure 9c shows that the viscosity distributions are similar to those in Figure 8, but the viscosity minimum reaches much lower values due to the effect of temperature, which in this case results in a further decrease in viscosity by another 3 orders of magnitude for an excess temperature of 400°C. This extremely low viscosity allows the material at the plume axis to achieve considerable velocity.

The relationships between buoyancy, velocity, radius, and entrainment are displayed in Figures 10 and 11 for $n=3$ and activation energies of 0 and 523 kJ/mol. As for the Newtonian rheologies, axial vertical velocity and plume radius increase, while entrainment decreases, with increasing buoyancy flux in the non-Newtonian cases. Velocities range from 30 cm/yr to 10 m/yr and radii vary from 50 to 150 km in the purely stress-dependent rheology. For the olivine rheology ($n=3$, 523 kJ/mol), velocities range up to nearly 100 m/yr at the highest temperatures, with similar radii.

Depth-Dependent Properties

Recent high-pressure experiments have suggested that thermal diffusivity may increase with depth in the Earth's

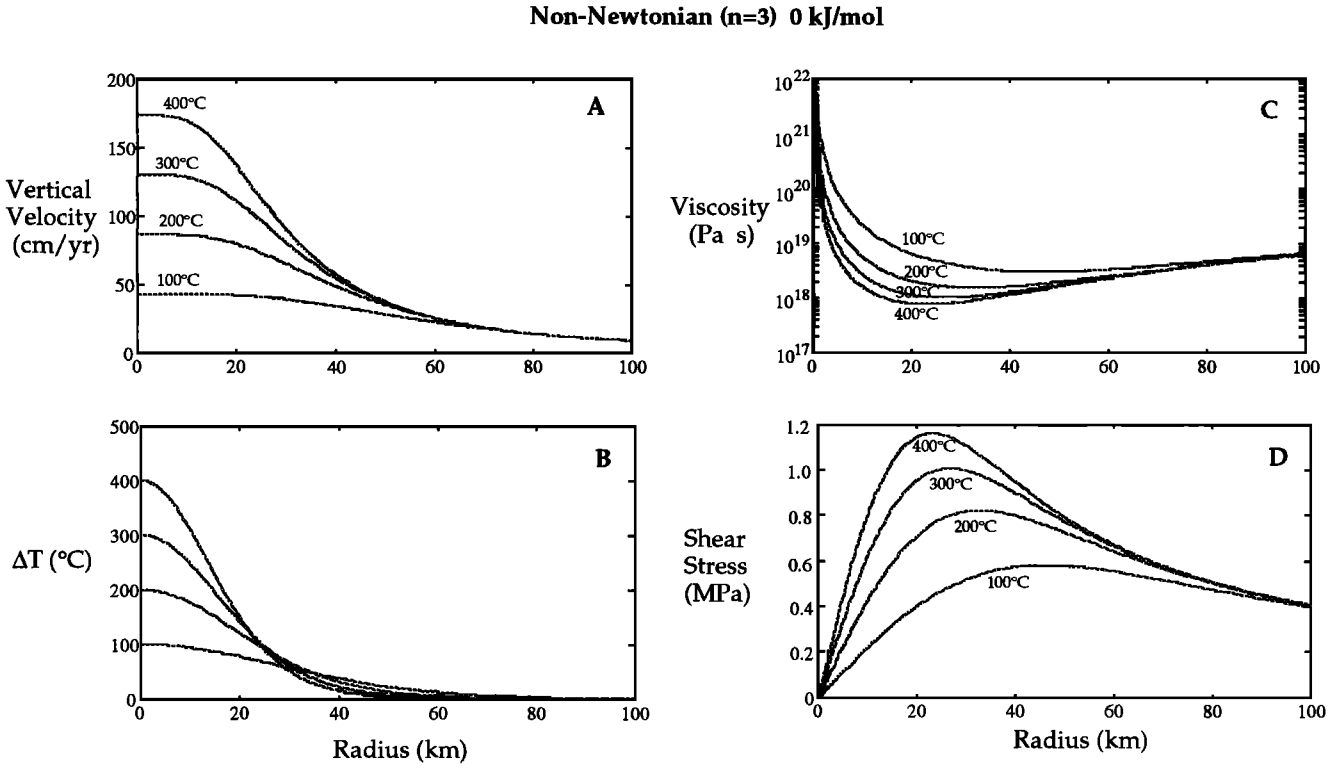

Figure 8. (a) Vertical velocity, (b) excess temperature, (c) viscosity, and (d) shear stress as a function of radius for n=3, 0 kJ/mol rheology. Velocity profiles show "plug flow" characteristic of non-Newtonian rheologies with n>1. This is due to very high viscosities at the plume axis, the result of low shear stresses in this region.

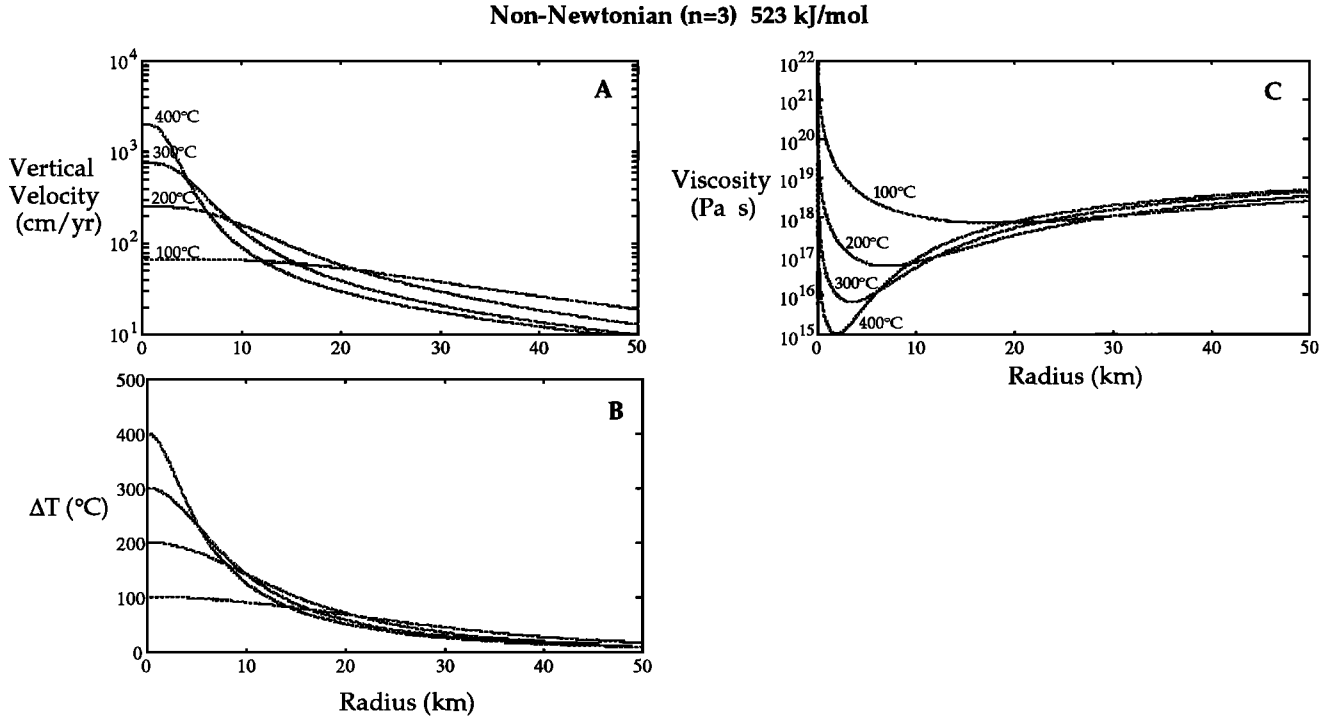

Figure 9. (a) Vertical velocity, (b) excess temperature, and (c) viscosity as a function of radius for n=3, 523 kJ/mol rheology. Minima in the viscosity profiles result from the competing effects of increasing shear stress (lowering viscosity) and decreasing temperature (increasing viscosity). The additional effect of temperature on viscosity results in viscosity drops of 3 to 6 orders of magnitude relative to the ambient viscosity. Plume radii, defined as 1% of axial ΔT, are off scale to right at 70 to 110 km.

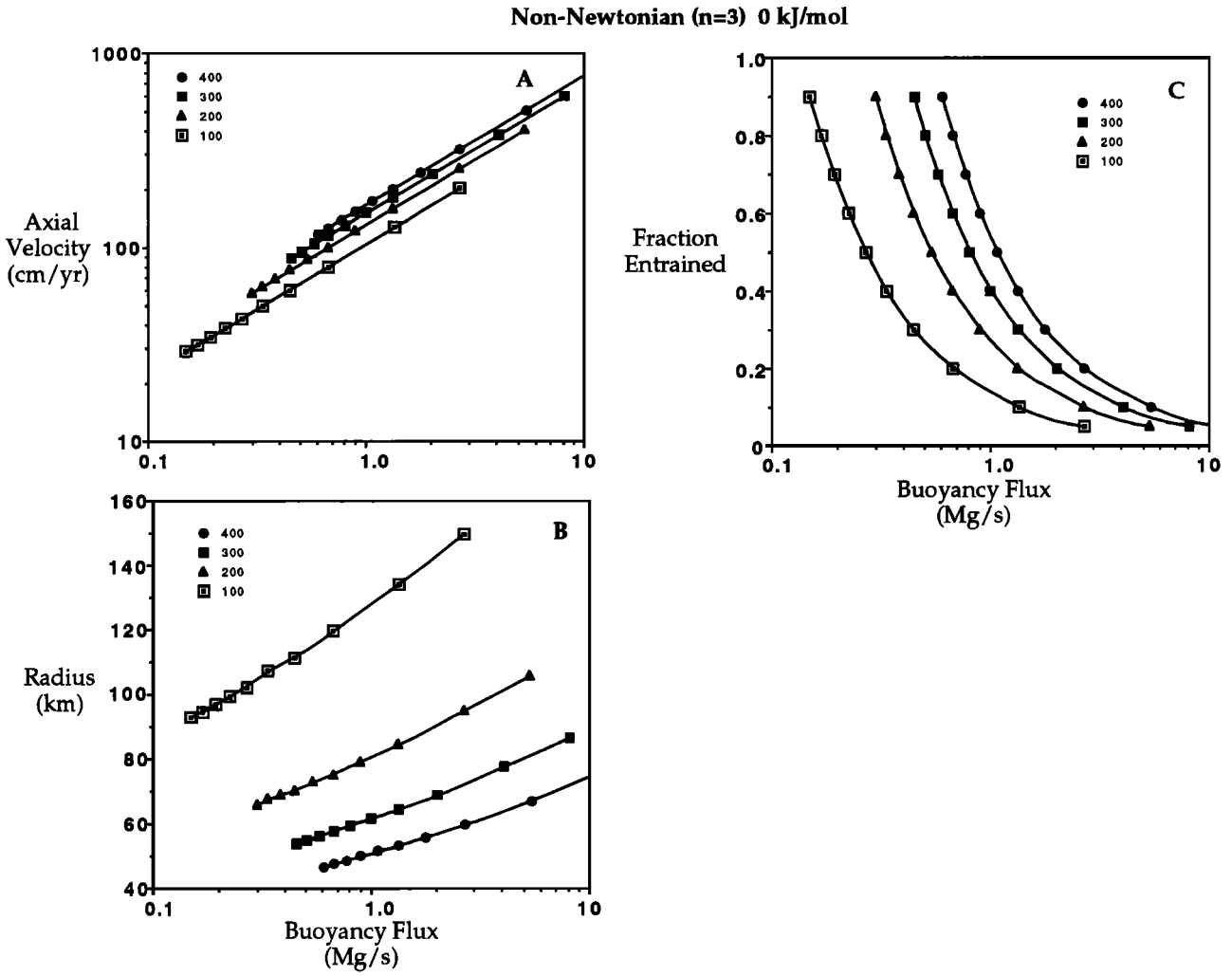

Figure 10. (a) Axial vertical velocity, (b) plume radius, and (c) amount of entrainment versus buoyancy flux for n=3, 0 kJ/mol rheology. Plume velocities are much higher, and radii much smaller, compared to the equivalent Newtonian cases without temperature-dependent viscosity (Figure 4).

mantle [*Osako and Ito*, 1991]. Since we have assumed that thermal diffusivity is constant (A8), we cannot model the depth dependence of this parameter, so the n=1, 523 kJ/mol case was modeled with a 10 times lower thermal diffusivity of 10^{-7} m^2/s. In Figure 12, these results are compared to the previous n=1, 523 kJ/mol case with $\kappa=10^{-6}$ m^2/s. From these figures, it is obvious that thermal diffusivity has a large influence entrainment. All else being the same, the most significant effect of decreasing thermal diffusivity from 10^{-6} to 10^{-7} m^2/s is to decrease entrainment substantially at a given buoyancy flux. Comparing plumes with similar buoyancy fluxes, it is apparent that those plumes with lower thermal diffusivities have much lower amounts of entrainment. This observation indicates that radial diffusion of heat is the main driving force for entrainment of ambient mantle, and this analysis suggests that there is a one-to-one correlation between thermal diffusivity and buoyancy flux. Since buoyancy flux is simply the excess temperature times the mass flux, we can see that higher thermal diffusivities promote the entrainment of more mass into plume conduits for a given temperature excess.

Recent high-pressure experimental studies have also shown that many materials, including olivine, exhibit decreases in thermal expansivity with increasing density [*Chopelas and Boehler*, 1989], and suggest that thermal expansivity may decrease by a factor of 6 to 20 across the full depth of the mantle. Incorporation of a depth dependent thermal expansivity (factor of 6 decrease, Figure 13b) shows essentially the same velocities and radii at a given buoyancy flux and ΔT_{top}, at the top of the plume, compared to the depth-invariant case (see Figure 5), due to the matching of the depth-dependent and constant thermal expansivities at the top of the plume. Axial velocities decrease with depth as thermal expansivity decreases. However, in the depth-dependent case, buoyancy flux increases with thermal expansivity from the base of the plume to the top.

Pressure and density considerations suggest that the mean viscosity of the mantle should increase with depth, so a factor of 100 depth increase in viscosity was incorporated into the n=1, 523 kJ/mol rheology (Figure 13c). The viscosity at the top of the plume is matched to 10^{21} Pa s, identical to the depth-invariant cases, whereas the ambient viscosity at the base of the plume is 10^{23} Pa s. The influence of temperature on viscosity remains the same. Again, the plume velocities,

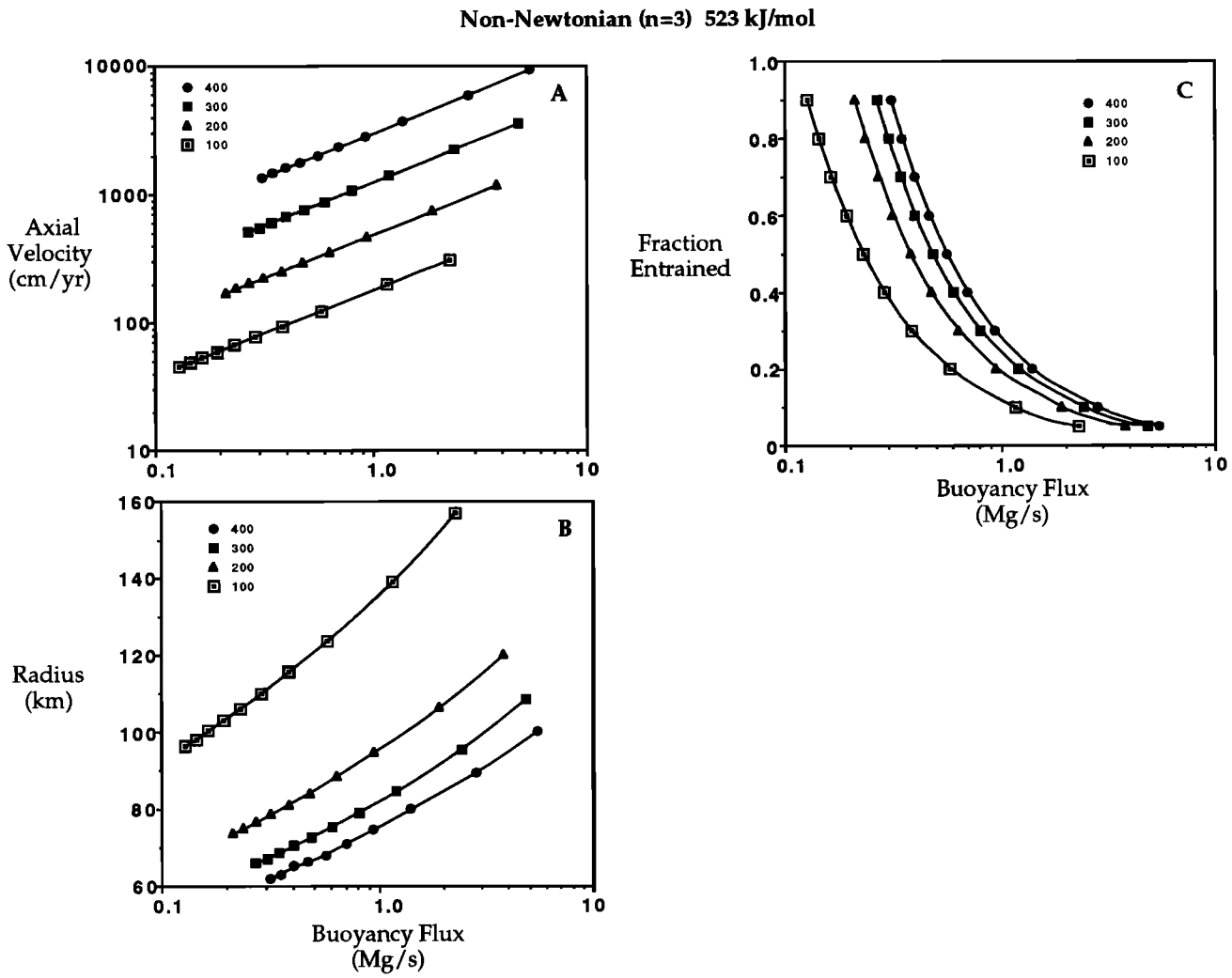

Figure 11. (a) Axial vertical velocity, (b) plume radius, and (c) amount of entrainment versus buoyancy flux for n=3, 523 kJ/mol rheology.

radii and entrainment as a function of buoyancy flux at the top of the plume are essentially the same as the depth invariant case (see Figure 5). With increasing depth, the vertical velocities decrease, and the plume radii increase, due to the increased viscous resistance to the plume flow. However, the slow flow in the lower half of the plume results in more entrainment of ambient mantle in this region, compared with the upper half of the plume (Figure 13c). For both viscosity and thermal expansivity, the most significant deviations from the depth invariant cases occur at depth, where the depth dependent values are most different from the reference values of the shallow mantle.

A Model for the Hawaiian Plume

The best current estimates of the physical state of the mantle suggest a Newtonian temperature-dependent rheology, a thermal expansion which decreases roughly by a factor of 6 through the mantle, and a corresponding increase of the mean viscosity, possibly by a factor of 100. The characteristics of hotspot swells and the petrology of plume basalts suggest an average excess temperature of about 200°C at hotspots [*Sleep*, 1990; *Albarede*, 1992], which translates into a maximum excess temperature of 400°C on the axis of a mantle plume. The best recent estimates for the temperature drop across D" stand at about 1300°C [*Boehler*, 1993]. However, it is not likely that this entire temperature excess is transported to the base of the plume conduit; a maximum excess temperature of 440°C was used to construct the plume model shown in Figure 14. The maximum axial velocity is 9.6 m/yr at the top of the plume, and the radius of the thermal field is about 40 km. Due to the depth dependence of thermal expansion and viscosity, this radius expands with depth to about 170 km. The hottest part of the plume, which would be seismologically observable, is restricted to a 20 km radius at the top, and a 60 km radius at the base of the plume, well within the thermal halo which defines the plume boundary. The buoyancy flux is 4.3 Mg/s, which is very similar to the latest estimates for the Hawaiian hotspot [*Ribe and Christensen*, 1994], and the entrainment is 9%. In order to match the Hawaiian buoyancy flux with a peridotite rheology, it is necessary to assume that the plume does not lose much excess heat on axis (about 40°C).

Our results have important implications for seismic and numerical convection studies concerned with mantle plumes. It is apparent that the small radii and large velocities of the plumes in this study, with realistic temperature- and stress-dependent rheologies, create problems of resolution and

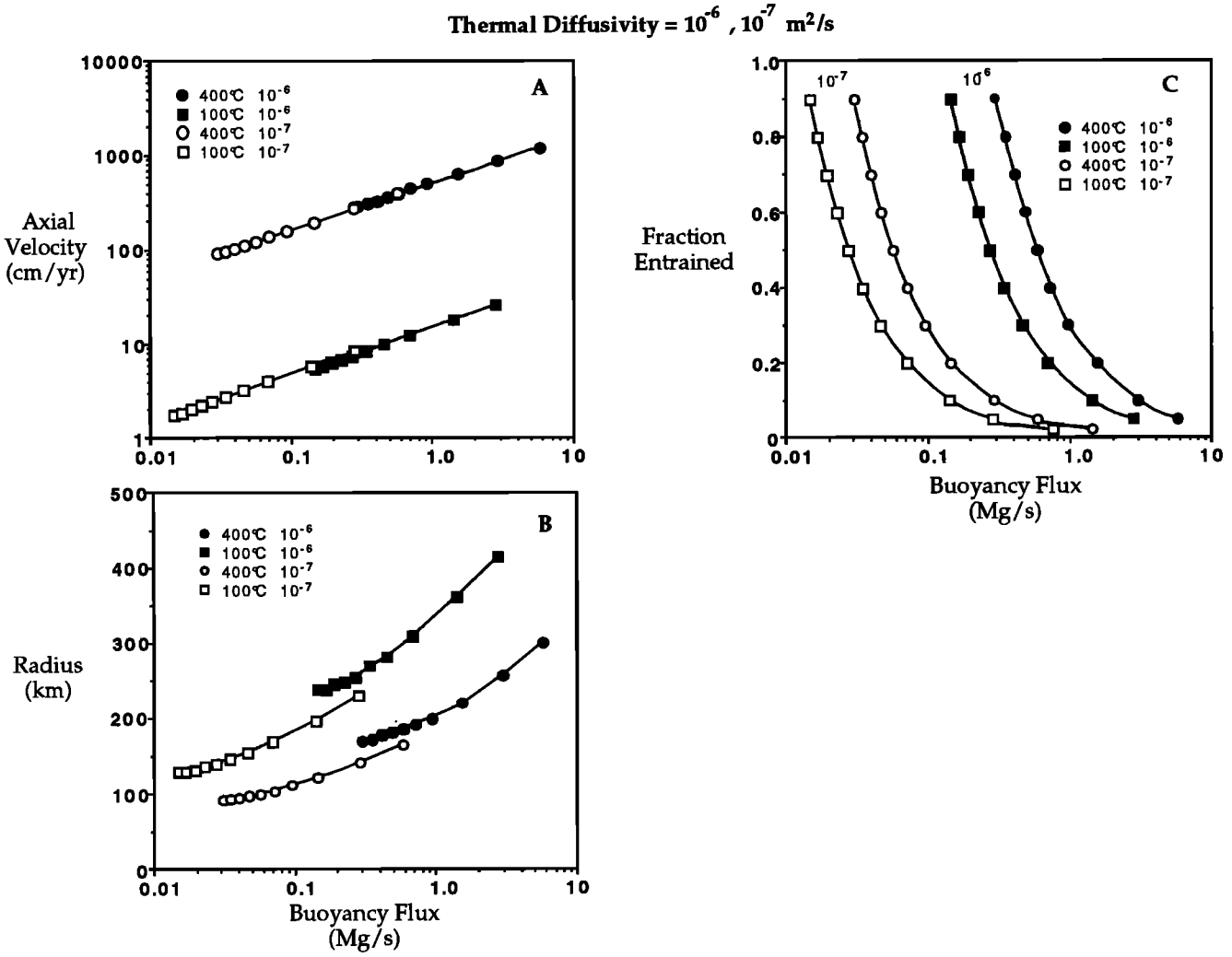

Figure 12. (a) Axial vertical velocity, (b) plume radius, and (c) amount of entrainment versus buoyancy flux for plumes with n=1, 523 kJ/mol rheology with ΔT_{top}=100°C (squares) and 400°C (circles), comparing the effects of differences in thermal diffusivity (10^{-6} m^2/s solid symbols, 10^{-7} m^2/s open symbols). A factor of 10 lower thermal diffusivity results in a large decrease in entrainment for a given buoyancy flux, with corresponding decreases in velocities and radii.

convergence for current efforts in large-scale numerical modeling of mantle convection, due largely to the effects of strongly variable viscosity. As a result, it is unlikely that large-scale models have accurately reproduced the sizes and velocities of plumes in the Earth's mantle, and have certainly not resolved flow within individual conduits which might facilitate studies of entrainment. Such small-scale features also will be very difficult to detect in most seismological situations, and will certainly fall through the cracks of whole planet tomographic inversions. In particular, high plume temperatures carry an inherent trade-off between larger slowness anomalies and smaller radii. It is likely that only the most favorable of conditions, such as the study of *Nataf and VanDecar* [1993] with dense ray coverage and low-noise receiver arrays, will be able to resolve mantle plume structures. However, due to the decrease of thermal expansion and increase of viscosity with depth, plumes are likely to be hotter and larger, and possibly more "visible" to seismic studies, near their source regions rather than at higher levels in the mantle.

Depths of Origin of Entrained Ambient Mantle

Structure of Plumes Undergoing Entrainment

From the above analysis, it is apparent that vertical, steady state plumes, with buoyancy fluxes comparable to mantle plumes in the Earth, will have mass fluxes consisting of 5 to 90% entrained, ambient mantle. If the plume experiences partial melting, this material will contribute some fraction of melt which may be erupted at the surface, and may contribute to the compositional variability of hotspot-related volcanics. Thus, the potential exists for identifying the geochemical signatures of plume source mantle and entrained ambient mantle, and in this respect, it becomes very important to constrain the original location of this entrained mantle.

Figure 15 shows the streamlines (light lines) and plume boundaries (heavy line) for three Newtonian, temperature-dependent plumes with n=1, activation energies of 523 kJ/mol, ΔT_{top}=400°C, and displaying different degrees of entrainment. The streamlines are observed to cross the boundary of the plume, and these plume boundaries increase

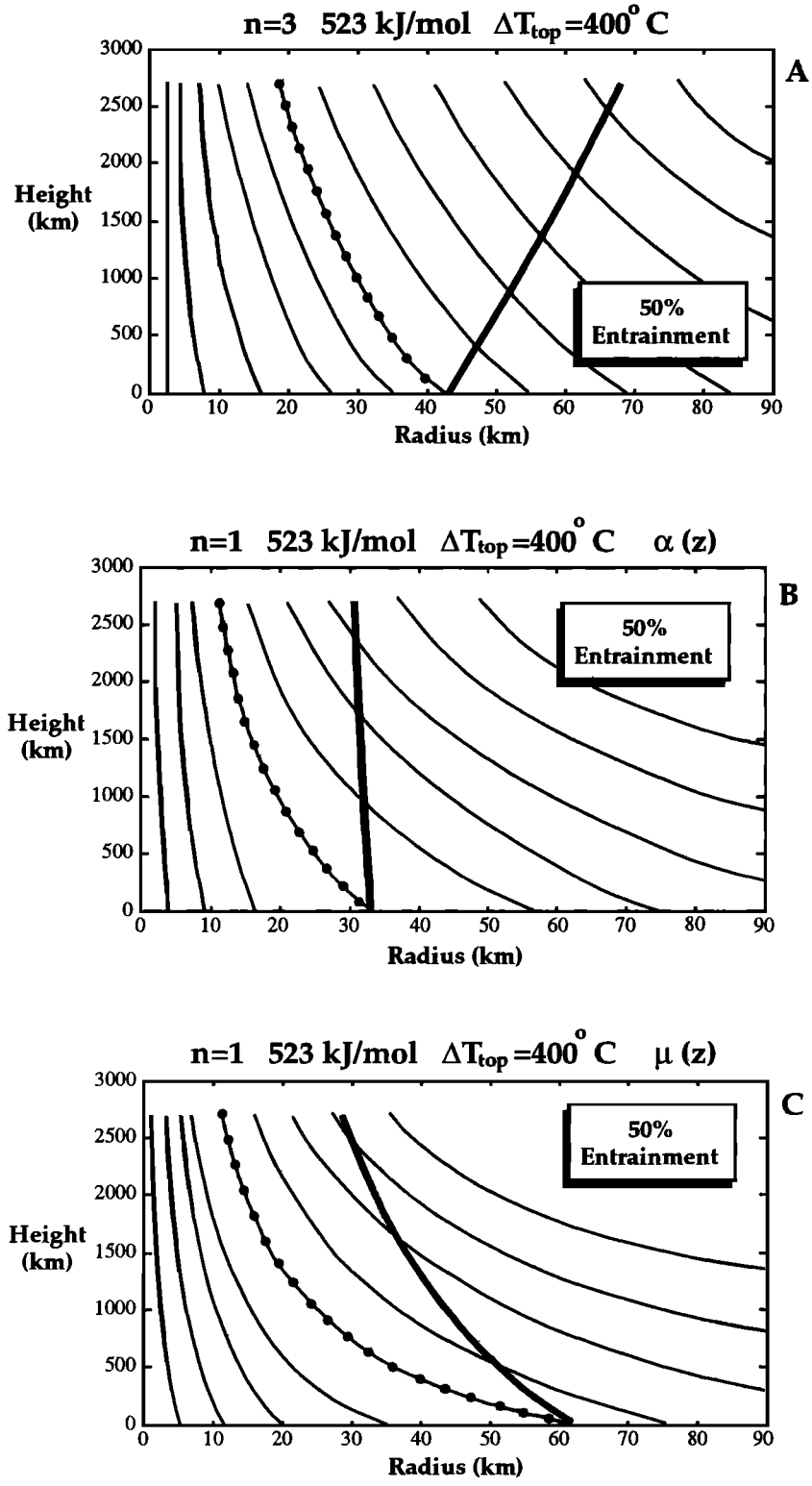

Figure 13. Streamlines for plumes of differing rheologies and physical properties, with ΔT_{top}=400°C and ΔT_{base}=800°C, resulting in 50% entrainment; (a) n=3, 523 kJ/mol rheology (s= -$^2/_3$), similar to the measured rheology of olivine; (b) n=1, 523 kJ/mol rheology with a coefficient of thermal expansion which decreases by a factor of 6 with depth (a=1.3, C_1=0.2133, s= -0.175); (c) n=1, 523 kJ/mol rheology with an ambient viscosity increase by a factor of 100 with depth (b= -3.7, C_2=0.288, s= -0.425). In all of these cases, these effects result in streamlines which are less vertical compared to the Newtonian cases in Figure 15. In addition, these streamlines become increasingly vertical with height, accentuating the entrainment of lower mantle material and exclusion of upper mantle material. The effects of increasing thermal expansion and decreasing viscosity with height results in acceleration of the plume velocities with height. These effects result in plume radii which tend to decrease with height (s>0).

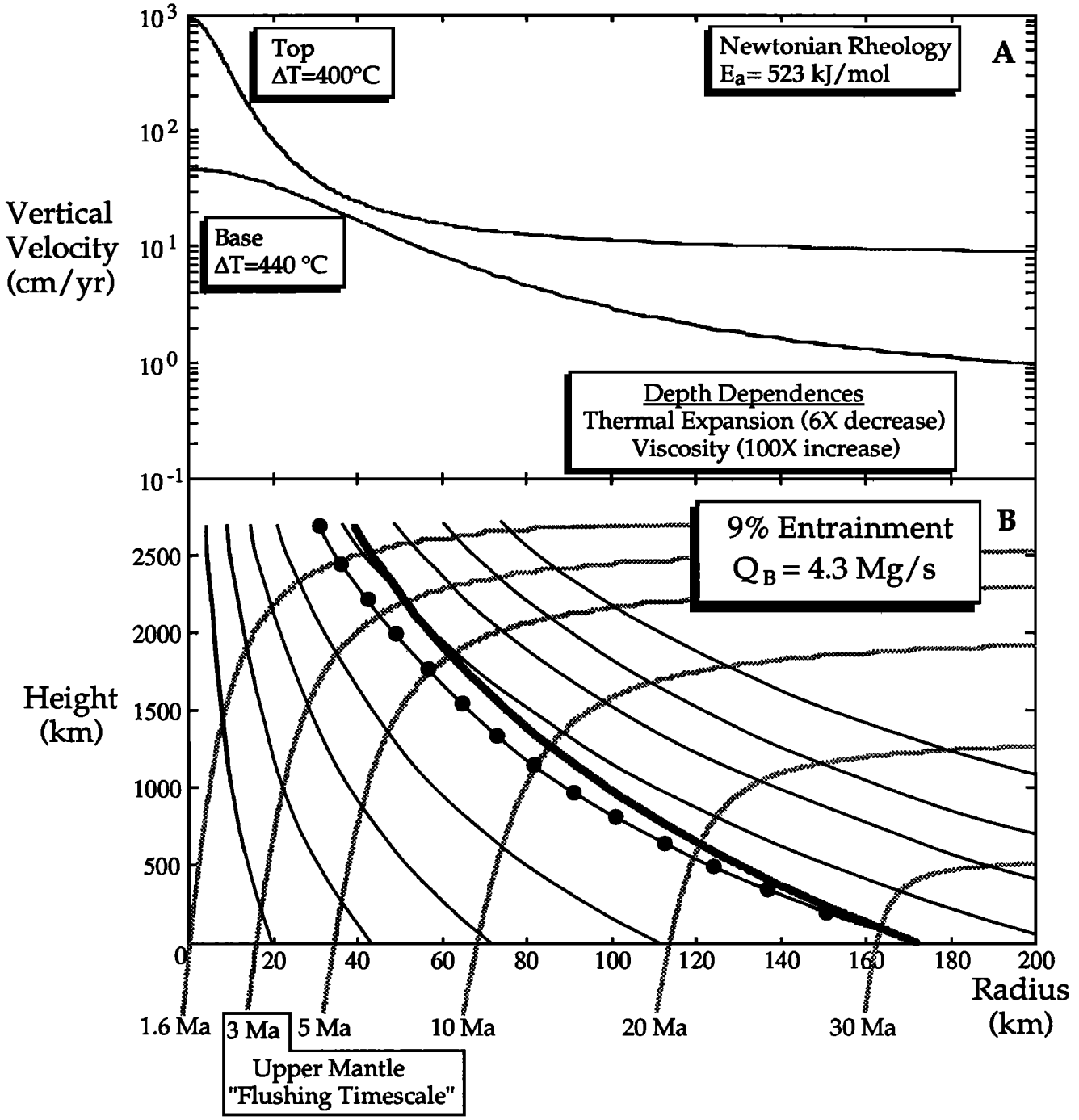

Figure 14. (a) Velocity profiles and (b) streamlines for a plume with Newtonian temperature-dependent rheology, and depth dependent thermal expansion (a=16, C_1=0.882, 6X decrease with depth) and viscosity (b=-42, C_2=0.896, 100X increase with depth). For ΔT_{base}=440°C and ΔT_{top}=400°C, the buoyancy flux is 4.3 Mg/s, very similar to the Hawaiian hotspot [*Ribe and Christensen*, 1994], and the entrainment is 9%. The vertical velocity at the top of the conduit approaches 10 m/yr. Dashed lines in Figure 15b are isochrons delineating the locus of fluid in the plume tracked back along a streamline for the indicated number of years. These isochrons show that, assuming initial representative entrainment (fraction of entrained upper mantle=9% x 670/2700), the upper mantle is flushed out of this plume conduit after 3 m.y. (upper mantle flushing timescale). This is similar to the lifetime of a single Hawaiian volcano, and much shorter than the lifetime of the Hawaiian hotspot.

with height due to the entrainment of ambient mantle. The dotted streamlines, which originate at the plume edge near the base of the plume, mark the boundary between the plume source mantle in the center, and the entrained ambient mantle at the periphery of the plume. Tracing these streamlines back into the far field, it is apparent that nearly all of the material which becomes entrained in the plume originates from the lowest levels of the system, largely from the lower half of the

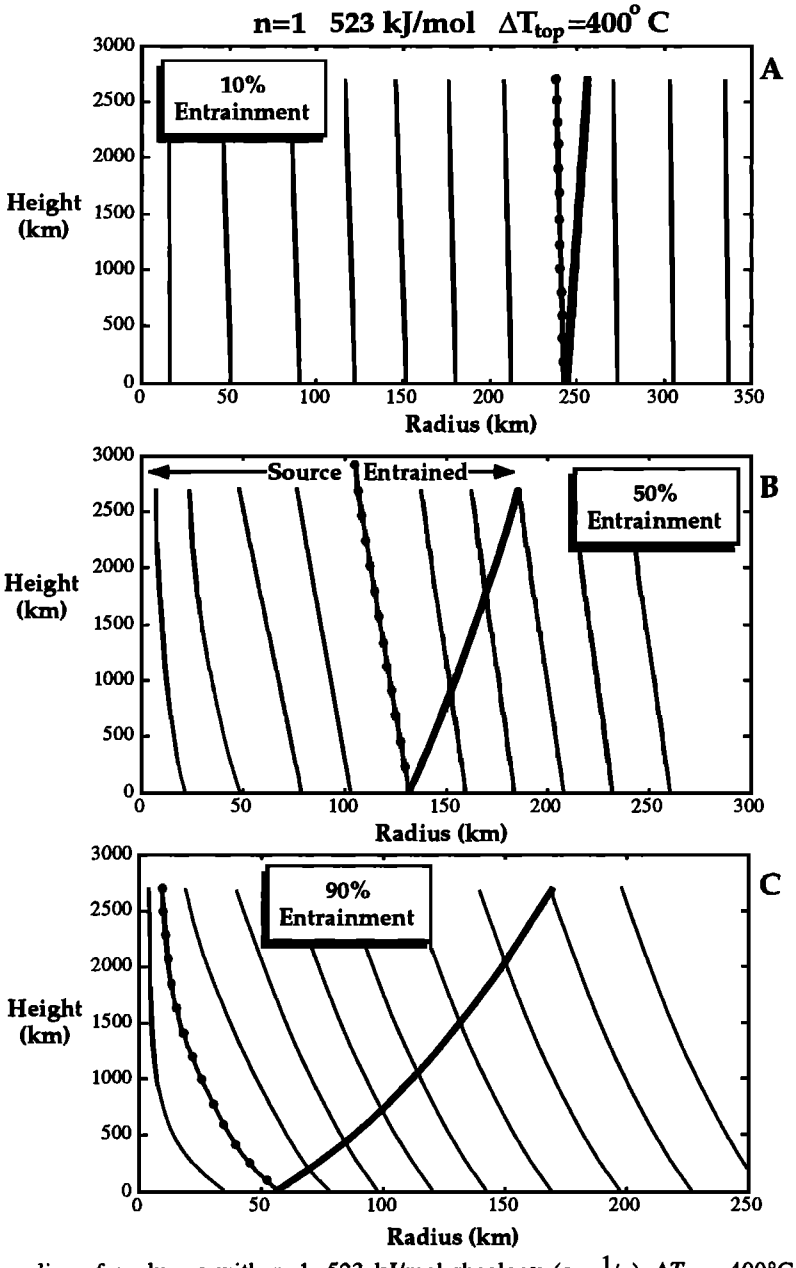

Figure 15. Streamlines for plumes with n=1, 523 kJ/mol rheology (s= -1/2), ΔT_{top}=400°C, and various amounts of entrainment (10% for ΔT_{base}=440°C, 50% for ΔT_{base}=800°C, 90% for ΔT_{base}=4000°C). Entrainment is shown by streamlines which cross the plume boundaries (heavy lines). Dotted streamlines mark the boundary between plume source and entrained mantle.

layer. The ambient mantle outside the thermal boundary consists of mantle derived from deep levels which has been dragged up around the plume by viscous coupling to the conduit flow.

The vertical nature of these streamlines is apparent in all the plumes studied. In Figure 13, streamlines are shown relative to plume boundaries for plumes with ΔT_{top}=400°C and ΔT_{base}=800°C, resulting in 50% entrainment. The three plumes represent three different cases, where n=3, 523 kJ/mol (Figure 13a); n=1, 523 kJ/mol, depth-dependent thermal expansivity (factor of 6 decrease) (Figure 13b); and n=1, 523 kJ/mol, depth-dependent viscosity (factor of 100 increase) (Figure 13c). In the non-Newtonian case (Figure 13a), the plume boundary still increases with height above the plume source, but for the depth dependent properties (Figures 13b and 13c), the plume radius decreases with height, even though mass flux increases with height. This is due to the upward acceleration of the fluid, driven by increasing thermal expansivity (Figure 13b) and decreasing viscosity (Figure 13c) with height above the plume source. In all three of these cases, the streamlines show that the mantle which is entrained across the plume boundary originates from the deepest levels of the fluid layer. Even though ambient mantle is still being entrained near the top of the plumes, by tracing streamlines back far enough in time, is apparent that this mantle originated from near the base of the system, largely from below 1200 km depth (1500 km height). Increasing viscosity and decreasing thermal expansion with depth will cause plume

flow to be slower in the lower mantle than in the upper mantle, allowing increased diffusion of heat, and thus entrainment of lower mantle material will dominate over upper mantle material.

A Timescale for Replacement of Entrained Upper Mantle

Hypothetically, if the plumes shown in Figures 13, 14, and 15 were to be instantaneously emplaced in the mantle, we might expect the streamlines to be horizontal in the far field, gradually relaxing to the steady state streamlines over time. In this horizontal streamline approximation, at the instant the plume was established, the plume would entrain ambient mantle in a representative manner along its entire length. In other words, the maximum amount of mantle which originated from above 670 km would be equivalent to 670/2700=25%, multiplied by the amount of entrainment. With time, as the streamlines relaxed to the steady state situation, this upper mantle material would be flushed out of the vertical conduit and be replaced by mantle derived from deeper levels. The maximum "flushing timescale" for the removal of all of the upper mantle material can be determined by calculating the time taken for mass to flow from 670 km depth to the top of the plume, along the streamline which crosses the plume boundary at a depth of 670 km (Figure 14). This upper mantle flushing timescale is displayed as a function of buoyancy flux in Figure 16b for the results of this study. Fields are shown which enclose all of the curves for the n=1 and n=3 cases (except the case with $\kappa=10^{-7}$ m^2/s). These timescales range from 0.4 to 4 Ma at the highest buoyancy fluxes, 1 to 10 Ma at a buoyancy flux of 1 Mg/s, and 7 to 70 Ma for the weakest plumes; if the plume boundary were to be defined closer to the plume axis, within the thermal halo, these timescales would be shorter by as much as an order of magnitude. For buoyancy fluxes >1 Mg/s, upper mantle flushing timescales are comparable to the lifetime of a given oceanic volcano, and much smaller than the age ranges observed for most linear island chains [*Duncan and McDougall*, 1976]. Within a given rheology, higher temperature plumes have higher velocities and thus smaller upper mantle flushing times, though the variation over the 400°C range of excess temperatures is small. The largest difference is that the plumes with non-Newtonian rheologies have systematically lower flushing times, due to their higher velocities.

In reality, these estimated timescales for flushing of entrained upper mantle from the conduits are probably too high, due to the approximations of instantaneous plume emplacement and horizontal streamlines. Numerous experimental studies [*Whitehead and Luther*, 1975; *Olson and Singer*, 1985; *Griffiths*, 1986] have documented that thermal plumes are generally initiated by a boundary layer instability which develops into a sub-spherical plume head. The time for formation and ascent of plume heads has been estimated at <100 Ma [*Sleep et al.*, 1988; *Griffiths and Campbell*, 1990]. The rise of this plume head through the mantle also drags up mantle from deeper levels and pushes away material above the sphere, deflecting streamlines upward. As a result of the rise of this starting plume, the trailing conduit is already surrounded by a sheath of mantle derived mostly from deeper levels, and by the time the plume head impacts the lithosphere, the amount of upper mantle material in the conduit is minimal. As a result, as long as the conduit remains

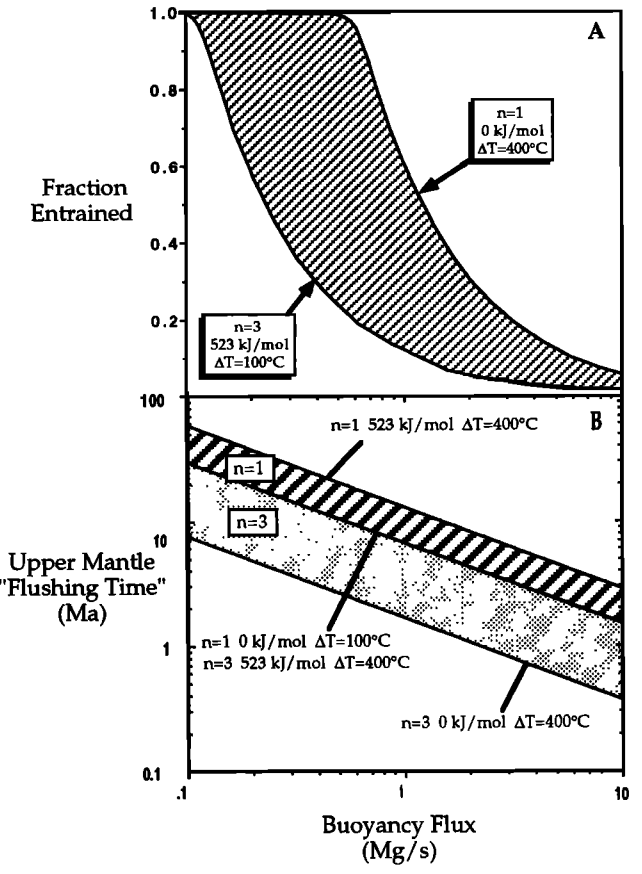

Figure 16. (a) Summary of entrainment versus buoyancy flux for plumes from this study. (b) Upper mantle "flushing times" for plumes from this study. Flushing time is defined as the time taken to remove all entrained upper mantle material from the plume conduit, assuming instantaneous emplacement of the plume and horizontal streamlines in the far field (see text). These times are likely to be upper limits, since mantle plumes are probably preceded by a larger head which sweeps up mantle from lower depths.

a continuous feature through the whole depth of the layer, the conduit will consist of a core of material from its source, surrounded by a region of entrained material which originated from the lower half of the fluid layer.

The primary constraint on entrainment derived from the present analysis is the location of origin of the fluid which is entrained. For physical properties which are constant with depth, and a viscosity which depends on temperature and shear stress, the fluid which is entrained into a thermally buoyant plume originates from near the base of the plume, and entrainment of fluid from the upper levels of the system is minor. The effect of increasing viscosity with depth in the ambient mantle is to reduce entrainment of fluid in the upper levels, due to the increase of the vertical velocity of the plume. This effect is also enhanced by a coefficient of thermal expansion which increases with plume height. If thermal diffusivity increases with depth, as suggested by recent experimental data [*Osako and Ito*, 1991], this would also indicate substantial entrainment of mantle at depth. Together, these effects indicate that the ambient mantle which is entrained into a vertical, contiguous mantle plume should

originate dominantly from the lower half of the layer traversed by the plume.

Geochemical Evidence for Entrainment

A New Model for Postshield Volcanism

Though the present analysis has concentrated on the dynamic structure of mantle plumes within the thermal field of the plume, a considerable amount of action takes place outside the plume boundary, in the ambient mantle which does not get heated and entrained. Examination of plume streamlines (Figures 7, 13, 14, and 15) shows that this material is also upwelling, due to viscous coupling to the flow in the plume conduit, and that at least some of this material originates from the upper mantle. This occurs even though the material is not heated by the plume. Figures 2, 3, 8, 9 and 14 indicate that the upwelling velocity of the mantle outside the plume boundary is typically 1 to 10 cm/yr, similar to upwelling velocities estimated beneath mid-ocean ridges [e.g., *McKenzie and Bickle*, 1988; *Sparks and Parmentier*, 1991; *Spiegelman and Elliot*, 1993]. This suggests that the ambient mantle outside the plume boundary will experience melting due to adiabatic decompression, generating a partial melt with a mid-ocean ridge basalt (MORB) isotopic signature. It is precisely this isotopic signature which is observed in alkalic basalts erupted on many oceanic islands after the main stage of shield building, and which has almost uniformly been attributed to melt interaction with the depleted mantle lithosphere [*Chen and Frey*, 1985; *Stille et al.*, 1986; *West et al.*, 1987; *Kurz et al.*, 1987; *Kennedy et al.*, 1991]. Upwelling rates of the mantle surrounding plumes suggests a plausible alternative to this model, which is that alkalic post-shield volcanics are generated by passive upwelling of the asthenospheric upper mantle. The passive upwelling of asthenosphere is driven by viscous coupling to the flow within the mantle plume (Figure 14), and by analogy with mid-ocean ridges, should generate a substantial amount of melt. Magma production rates would be considerably higher than within the conductively heated, depleted lithosphere. The main difference is that this melt will be generated mostly at high pressures within the stability field of garnet lherzolite, resulting in alkalic magmas with upper mantle (MORB) isotopic signatures. Close to the plume, these magmas will be diluted by the extensive amounts of plume melting; however, these melts could be important components of the magmas erupted away from the plume axis, including post-shield volcanics. This model would predict a significant amount of volcanism off the axis of the Hawaiian ridge. In fact, extensive alkali basalt sheet flows with MORB-like isotopic compositions have recently been discovered 200 km south of Hawaii [*Lipman et al.*, 1989] and 200 km north of Oahu and Kauai [*Clague et al.*, 1990]. The aerial extent of these lava fields are comparable to the subaerial exposures of the Hawaiian Islands.

Entrainment and Mixing in Mantle Plumes

Isotopic data for OIB and MORB have provided most of the evidence for the chemical heterogeneity of the convecting mantle. Based on the fluid dynamic analysis presented here, it may be possible to decipher some signal in the isotopic data for hotspot volcanics which may be related to entrainment. Figure 17 shows a projection of a three-dimensional plot of the currently available data for $^{87}Sr/^{86}Sr$, $^{143}Nd/^{144}Nd$ and $^{206}Pb/^{204}Pb$ for oceanic basalts, modified from *Hart et al.* [1992]. The entire data cloud is mostly enclosed by a tetrahedron, the corners of which correspond to end-member isotopic compositions described by *Zindler and Hart* [1986]. The depleted MORB mantle (DMM) is the source of MORB present in the uppermost mantle, HIMU is a high-$^{206}Pb/^{204}Pb$ component which may be related to recycled oceanic lithosphere [*Hofmann and White*, 1980; *Chase*, 1981; *Hauri and Hart*, 1993], and EMI and EMII are enriched mantle compositions which may be related to recycled sediments [*White and Hofmann*, 1982; *Wright and White*, 1987; *Woodhead et al.*, 1993] or continental lithosphere [*McKenzie and O'Nions*, 1983].

In Figure 17, fields enclose data from several islands or island chains which are characterized by linear arrays suggestive of two-component mixing. For most island chains, the data are not randomly positioned within this three-dimensional space [*Hart et al.*, 1992]. In fact, there is a notable lack of mixing arrays joining the EMI, EMII and HIMU apices of the tetrahedron. In our estimation, this observation would seem to rule out a random mixing process such as bulk convective mixing, which would not discriminate between different mantle compositions. Instead, the arrays are systematically oriented within isotope space, originating from points at various locations along the EMI-HIMU and EMII-HIMU joins, and converging on a volume in Sr-Nd-Pb isotopic space which is clearly different from the depleted MORB mantle (DMM) end-member, and distinct from the sources of typical N-type MORB [*Hart et al.*, 1992]. This distinction is most evident in the isotopic compositions of Pb and He. Existing He isotope data for these island chains show a clear increase in $^{3}He/^{4}He$ moving along the arrays toward the region of convergence, though these arrays do not converge toward a single characteristic value of $^{3}He/^{4}He$. However, the arrays are sublinear in four-dimensional He-Sr-Nd-Pb space. Other islands which display high $^{3}He/^{4}He$ ratios are characterized by Sr, Nd and Pb isotope signatures which plot near this region. These features of the hotspot isotope data indicate the presence of a widespread component in the convecting mantle, which is appearing at hotspots around the world. This component, termed FOZO by *Hart et al.* [1992], is not very well defined by the available data, but its approximate range of composition is $^{87}Sr/^{86}Sr$ of .7030-.7040, $^{143}Nd/^{144}Nd$ of .51300-.51280, $^{206}Pb/^{204}Pb$ of 18.50-19.50, $^{207}Pb/^{204}Pb$ of 15.55-15.65, and $^{208}Pb/^{204}Pb$ of 38.8-39.3 with elevated $^{3}He/^{4}He$ (>8 Ra). The FOZO ends of these arrays show variable $^{3}He/^{4}He$ ratios of 8-15 Ra, with the notable exceptions of Iceland (22 Ra), Hawaii (32 Ra) and Samoa (24 Ra).

Two aspects of the isotope data should be emphasized. First, the arrays in Figure 17a originate from points near the EMI-HIMU and EMII-HIMU joins, and not from the EMI-EMII join, nor from locations central to the EMI-EMII-HIMU triangle. This observation indicates that there is some process which results in juxtaposition of the EMI and EMII components with HIMU, and which predates mixing with FOZO [*Hart et al.*, 1986]. Based on arguments noted previously that these components may be related to modern sediments (EMII), ancient sediments or strongly depleted lithosphere (EMI), and recycled oceanic crust (HIMU), there is a strong possibility that the relationship of EMI and EMII with HIMU may relate to the sediment-basalt-harzburgite layering of the oceanic lithosphere as it is subducted. Second, the convergence of the Sr-Nd-Pb-He isotope data toward FOZO strongly suggests the

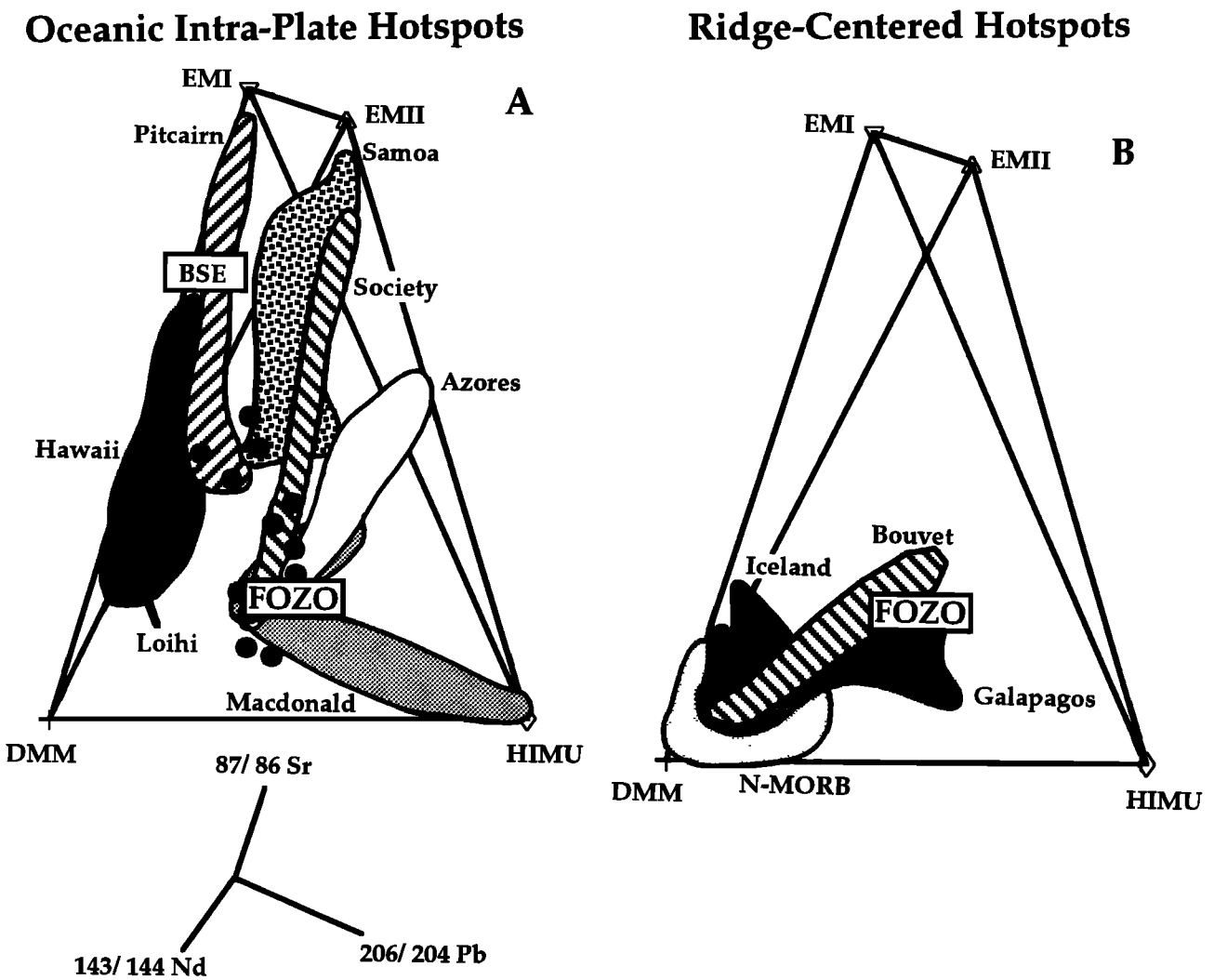

Figure 17. Three-dimensional plot of $^{87}Sr/^{86}Sr$, $^{143}Nd/^{144}Nd$ and $^{206}Pb/^{204}Pb$ for oceanic basalts worldwide, modified after *Hart et al.* [1992]. The data are enclosed by a tetrahedron, with the apices defined by the end-members of *Zindler and Hart* [1986]. (a) Fields enclose data for selected hotspot islands and island chains which show elongate arrays. These arrays converge on a volume in isotope space (FOZO) which is distinct from mid-ocean ridge basalts (MORB) and is characterized by high $^{3}He/^{4}He$ ratios, indicating the presence of a volumetrically important component common to hotspots worldwide, and which is probably the lower mantle. (b) Fields enclose data for selected ridge-centered hotspots, showing mixing trends with the upper mantle MORB source. Bouvet and Galapagos fields extend from the MORB field toward FOZO.

existence of a mantle component which is common to hotspots worldwide and, as such, probably represents a substantial volume of mantle distinct from the source of MORB. In fact, only hotspots within a few hundred kilometers of the mid-ocean ridges show a component of MORB source mantle in their shield-building volcanics (Figure 17b). The observation that intraplate hotspots show no mixing with MORB mantle is consistent with the prediction from entrainment theory that entrainment of uppermost mantle should be insignificant in mantle plumes. This absence of upper mantle entrainment would seem to be inconsistent with the model for entrainment in an inclined plume conduit [*Richards and Griffiths*, 1989; *Griffiths and Campbell*, 1991], since the sharpness of the bend in the Hawaii-Emperor Seamount chain essentially requires that the inclination of the plume conduit take place in the uppermost mantle [*Richards and Griffiths*, 1989].

In the context of the present results, if FOZO does in fact have high $^{3}He/^{4}He$, then it may be suggested that an origin for plumes from a thermal boundary layer at 670 km depth can be discounted. If such plumes existed, they would be expected to consist largely of depleted upper mantle, or at the very least entrain upper mantle and show some mixing toward MORB, which is clearly not observed in Figure 17 (with the exception of ridge-centered hotspots). If FOZO is associated with a boundary layer at 670 km (instead of core-mantle boundary), then plumes with FOZO as a component should still show mixing toward MORB, since it is the downward motion of the upper mantle which would replenish material in a 670 km thermal boundary layer. Even if the boundary layer were made up largely of subducted oceanic crust, such sinking cold plumes should still entrain upper mantle material due to the lateral conduction of "coldness," in much the same manner as hot plumes entrain ambient mantle. Thus the location of

FOZO in the mantle above 670 km is deemed unlikely due to the absence of a MORB signature in intraplate hotspots, and the absence of a high $^3He/^4He$ signature in N-type MORB. Since it is unlikely that an origin for mantle plumes in a 670 km boundary layer can be reconciled with the presence of a high $^3He/^4He$ FOZO, this provides support for plume transport across the 670 km discontinuity.

Mantle Plumes as Probes of the Lower Mantle

The binary nature of these arrays begs the question as to which components are present in the plume source, and which components are entrained. Due to the lack of high $^3He/^4He$ signatures in MORB, high $^3He/^4He$ indicates a source which is distinct from the uppermost mantle, most probably the lower mantle [*Lupton and Craig*, 1975; *Craig and Lupton*, 1976]. Thus the high $^3He/^4He$ signature of FOZO would logically place this component in the lower mantle. However, the location of FOZO in the lower mantle does not provide a simple answer to whether FOZO is plume source mantle, or entrained mantle. For example, plumes are often proposed to originate from a thermal boundary layer at the core-mantle boundary [*Stacey and Loper*, 1983]. This requires that the thermal boundary layer be replenished to replace the mantle which is lost to mantle plumes. In the absence of the total population of the core-mantle boundary by subducted slabs, the core-mantle boundary layer (CMBL) would essentially be replenished by the downward motion of the lowermost mantle toward the core. Thus, if FOZO is present in the lower mantle, then it should also be present, at some level, in the CMBL. Two endmember scenarios are possible which would be consistent with the isotope data and the results from entrainment dynamics.

Model 1: FOZO represents lower mantle material in the CMBL, and enriched components are entrained as blobs from the lower mantle. This scenario would be consistent with a CMBL which contains only a small fraction of slabs, the remaining material being ambient lower mantle. If the lower mantle rheology exhibited a significant increase in viscosity with depth, this would provide increasing resistance to subduction of lithosphere to the CMBL. Thus, some slabs would instead be swept up in the background convective flow within most of the mantle, to be available for entrainment into mantle plumes. As a result, most of the mantle material in the CMBL would be lower mantle material conductively heated by the core.

Limited evidence in favor of model 1 comes from the observation that a strong FOZO signature in some island chains (all from the Pacific) seems to be connected with the most recent shield building volcanism within the chain. Loihi Seamount (Hawaii), Macdonald Seamount (Macdonald), Manu'a Islands (Samoa), and Mehetia Seamount (Society) all lie at the FOZO end of the data arrays (Figure 17). Most of these young volcanoes (Loihi, Mehetia, Macdonald) are characterized by $^3He/^4He > 9$ Ra [*Staudacher and Allegre*, 1989; *Desonie et al.*, 1991]. In addition, the highest $^3He/^4He$ data from Iceland comes from the southeastern neovolcanic zone, which became active only 1.5 Ma ago [*Kurz et al.*, 1985] and is the youngest of the three rift zones on Iceland. If the mantle at the plume axis is at the highest temperature, and is rising at the highest velocity, then melt production will be greatest at the axis of the plume, and these melts might be the dominant melt products at nascent volcanic features. This idea may be supported by the $^3He/^4He$ data from Loihi, in which the highest $^3He/^4He$ ratios come from tholeiitic basalts representing large degree melts (26-32 Ra), and a basanite, representing a small degree melt, records the lowest Loihi value (20 Ra) [*Kurz et al.*, 1983]. At Samoa, however, *Farley et al.* [1992] have measured $^3He/^4He$ values of 12-25 Ra within a single exposure of shield flows from the island of Tutuila, which indicates the complexity of this problem.

Model 2: the enriched components (EMI, EMII, HIMU, and intermediate compositions) are located in the CMBL, and FOZO represents entrained lower mantle. This model suggests that the CMBL is populated largely by recycled slabs, and any material they have entrained during slab transport. We favor this model because it is consistent with a number of geochemical and geophysical observations. Evidence for the presence of both FOZO and pure end-member components in the same hotspot system exists in the isotope data for the Hawaiian Islands (EMI), Samoa (EMII) and the Macdonald hotspot chain (HIMU), indicating that all of the enriched end-member components must be available for mixing with FOZO in the lower mantle. To make the CMBL and the lower mantle isotopically distinct would require some process which transports material in a relatively pure state through the mantle to the CMBL, whereupon it is incorporated into mantle plumes. Since EMI, EMII and HIMU may all represent components which may be subducted with the oceanic lithosphere, this model is consistent with recent analyses of the Earth's D" layer which indicate that this boundary layer may not be entirely thermal [*Young and Lay*, 1987; *Wysession*, 1993; *Stevenson*, 1993]. This model is also consistent with recent planetary-scale studies of mantle convection in which slab material is temporarily trapped at the 670-km discontinuity, and episodically transported to the base of the lower mantle in the form of catastrophic avalanches [*Christensen and Yuen*, 1985; *Machetel and Weber*, 1991; *Peltier and Solheim*, 1992; *Tackley et al.*, 1993].

In addition to mixing and entrainment effects during plume transport, the entrainment signature might be overprinted by a change in the composition of the plume source at the CMBL. For example, the isotopic compositions of the basalts along the Macdonald hotspot chain change abruptly from endmember HIMU compositions (Mangaia, Rurutu, Tubuai, 20 to 6 Ma) to compositions intermediate between HIMU and EMII (Rapa, Macdonald Seamount, 6 Ma to the present), both of which converge near the center of the isotope tetrahedron (Figure 17). The ages of volcanics from the islands of Tubuai and Rapa overlap at about 7 Ma, indicating that these two islands, in the same island chain, were simultaneously erupting basalts with very different isotopic compositions. This seems to require an abrupt change in the isotopic composition of the mantle being supplied by the plume. Because of these complications, it is not yet possible to determine whether the boundary layer sources of plumes contain entirely FOZO or entirely enriched components. It is possible that both FOZO and the enriched components may be present, depending on the dynamics and history of the thermal boundary layer itself beneath individual plumes [*Sleep*, 1992].

Speculation on the Evolution of the Lower Mantle

High $^3He/^4He$ has previously proposed to be associated with primitive, or undifferentiated mantle. The Sr-Nd-Pb isotopic composition of FOZO, however, is clearly different from proposed "bulk silicate Earth" isotopic compositions [*Zindler*

and Hart, 1986]. In particular, the depleted Nd isotope signature of FOZO suggests long-term depletion in the light rare earth elements, and the Pb isotope signature does not plot on a 4.56 Ga geochron as it should if the lower mantle has been a closed system for 4.56 Ga. There are two main ways in which the lower mantle can evolve to the present isotopic composition of FOZO.

First, relative to the upper mantle source of MORB, the Sr and Nd isotope signatures of FOZO are only slightly less depleted than the upper mantle, which may be an indication that the same process (i.e., extraction of the continental crust) has operated to different degrees on both reservoirs. If the bulk peridotite/melt partition coefficient for He is less than for U, as suggested by phenocryst/glass measurements [*Kurz*, 1993; *Marty and Lussiez*, 1993], then the upper mantle would have a lower $^3He/^4He$ ratio than FOZO, as is observed. This scenario would favor a convective regime with substantial mass exchange between the upper and lower mantles.

Mantle plumes may facilitate this exchange. Assuming an average plume temperature of 200°C, the analysis of *Sleep* [1990] suggests a global plume mass flux of $2.9x10^{14}$ kg/yr. If 25% of this flux is entrained lower mantle, the amount of lower mantle carried by plumes over the age of the Earth would amount to $3.2x10^{23}$ kg, or about 10% of the mass of the lower mantle. An equivalent mass of upper mantle or lithospheric material would be displaced into the lower mantle. This integrated mass of entrained material would make up 30% of the mass of the mantle above 670 km, and would replenish the supply of incompatible trace elements in the upper mantle after extraction of the continental crust. This type of mass exchange will serve to buffer the He and Pb isotopic composition of the upper mantle [*Galer and O'Nions*, 1985; *Kellogg and Wasserburg*, 1990]. The Pb isotope signature of FOZO, however, is not consistent with depletion of U and Th relative to Pb shown by the upper mantle [*White*, 1993], unless the U/Pb age of the earth were considerably younger than 4.56 Ga, such that FOZO would plot on, or to the left of, the Pb-Pb geochron.

However, an alternative origin for FOZO is possible. Though consistent with a layered mantle, the necessity of maintaining isotopically distinct upper and lower mantles does not require layered convection, but may instead be the result of different time constants of mixing for the upper and lower mantles. In this case, with limited exchange between the upper and lower mantles, it is possible that the difference in isotopic composition between FOZO and the upper mantle may be the time-integrated signature of Rb/Sr, Sm/Nd and (U,Th)/(Pb,He) fractionations resulting from differentiation of a terrestrial magma ocean early in the Earth's history. The isotopic distinction between FOZO and the upper mantle would then likely be a reflection of differences in the major element composition of the upper and lower mantles [*Agee and Walker*, 1988]. The current database of mineral/melt partitioning data for trace elements in majorite garnet, silicate perovskites and magnesiowustite is insufficiently precise to be able to evaluate this possibility, but this type of data will ultimately be the strongest test of this mode of planetary differentiation.

Conclusions

The point-source boundary layer model described here has allowed the high-resolution examination of the thermal, velocity, viscosity and shear stress structure within individual plume conduits. The model incorporates temperature- and stress-dependent rheologies, as well as a depth-dependent viscosity and thermal expansivity. Our model shows that, for realistic temperature- and stress-dependent rheologies, mantle plumes with buoyancy fluxes of 0.1 to 10 Mg/s should be exceedingly narrow features characterized by rapid upwelling rates (meters/year). However, these narrow plumes are surrounded by a larger thermal halo, within which mantle is still upwelling at considerable velocities (centimeters/year). Outside of the thermal halo which defines the plume boundary, ambient mantle is dragged up by viscous coupling to the plume flow, with upwelling rates of 1 to 10 cm/yr, similar to mid-ocean ridge upwelling rates. This upwelling is proposed as a mechanism to generate post-shield and post-erosional alkalic magmas, with MORB chemical affinities, found on many linear island chains.

Ambient mantle immediately surrounding plumes in entrained by the conduction of heat away from the plume conduit; this heat raises the buoyancy and lowers the viscosity of the ambient mantle to the extent that it becomes part of the conduit flow. All of the plumes examined in this study showed significant entrainment, and entrainment was found to correlate negatively with buoyancy flux. Thermal effects have the largest influence on the entrainment process; all else being equal, plumes with higher temperatures, more temperature-sensitive rheologies, and larger thermal diffusivities experience more entrainment. Stress dependence of the rheology, while significantly affecting plume velocities and radii, has very little effect on the amount of entrainment.

Analysis of the streamlines describing plume flow demonstrates that most of the mantle which is entrained into vertical, steady state plumes originates from the lower mantle, with very little upper mantle entrainment. Timescales for replacement of entrained upper mantle by entrained lower mantle range from 1 to10 Ma for plumes with buoyancy fluxes larger than 1 Mg/s. Increases in viscosity and thermal diffusivity and decreases thermal expansion with depth, only serve to enhance the entrainment of lower mantle material over upper mantle material. The Sr, Nd, Pb and He isotope database for hotspot volcanics clearly reflects the presence of a mantle component with depleted Sr and Nd isotopes, radiogenic Pb isotopes, and high $^3He/^4He$ ratios. This component (FOZO), being a nearly ubiquitous component present in hotspots around the world, probably represents a substantial volume of mantle; however, it is not the upper mantle source of MORB. This component is logically identified as the high $^3He/^4He$ lower mantle. The geochemistry of hotspot volcanics thus appears to provide independent evidence for the entrainment of lower mantle into mantle plumes. If FOZO does represent the composition of the lower mantle, then this reservoir has been chemically differentiated at some point in its past. This may have occurred through extraction of small amounts of melt at higher levels in the mantle, or through fractionation during differentiation of a terrestrial magma ocean during formation of the Earth. The former scenario would be consistent with whole mantle convection, on average; the latter would require some degree of convective layering.

Appendix: Derivation of the Boundary Layer Plume Model

This study examines the vertical, steady state boundary layer flow around a point source of heat in axisymmetric coordinates

(Figure 1). In this analysis, we are concerned only with the flow in a vertical, steady state conduit. In an incompressible Boussinesq fluid, the boundary layer equations used are modified after *Schlichting* [1968]:

$$\frac{\partial}{\partial Z}(UR)+\frac{\partial}{\partial Z}(VR)=0 \tag{A1}$$

$$U\frac{\partial T}{\partial Z}+V\frac{\partial T}{\partial R}-\frac{\kappa}{R}\frac{\partial}{\partial R}\left(R\frac{\partial T}{\partial R}\right)=0 \tag{A2}$$

$$\frac{1}{R}\frac{\partial}{\partial R}(\tau_{ZR}R)+\rho g\ \alpha_o\left(C_1\frac{Z}{h}\right)^a\Delta T=0 \tag{A3}$$

where ΔT is the difference between the temperature inside the plume (variable) and the temperature in the ambient fluid (constant). The rheological equation of state is assumed to be of a form similar to that given by *Yuen and Schubert* [1976]:

$$\tau_{ZR}=\left[M\left(C_2\frac{Z}{h}\right)^b F(\Delta T)\frac{\partial U}{\partial R}\right]^{\frac{1}{n}}. \tag{A4}$$

The definitions of the various parameters are given in Table 1. In these equations, thermal diffusivity is constant, but thermal expansivity (α) and the preexponential factor for viscosity (M) are allowed to vary with depth, or in practice, with height (Z) above the point source relative to a characteristic scale length (h). The constants (C_1, a) determine the depth variation of α, and the constants (C_2, b) determine the depth variation of M. In (A4), the strain rate is given by the gradient of vertical velocity in the radial direction [*Yuen and Schubert*, 1976], and $F(\Delta T)$ is a term which describes the dependence of the viscosity on excess temperature. Typically, $F(\Delta T)$ is given by an Arrhenius relationship for temperature

$$\exp\left(\frac{E_a+pV_a}{RT}\right) \tag{A5}$$

where R is the gas constant, p is pressure, and E_a is the activation energy and V_a the activation volume for viscous flow. However, a similarity solution is not possible for the above equations if (A5) is used for $F(\Delta T)$. Instead, the temperature dependence of the rheology is given by an empirical relationship:

$$F(\Delta T)=\exp\left(\exp\left(\exp\left(\exp\left[A-B\left(\frac{Z}{h}\right)\Delta T\right]\right)\right)\right)$$
$$=^4\exp\left[A-B\left(\frac{Z}{h}\right)\Delta T\right]. \tag{A6}$$

In this parameterized temperature-dependence term, the number of nested exponentials, as well as the constants A and B, can be fit to an Arrhenius function for viscosity for any activation energy (Figure A1), and is a function of ΔT relative to the ambient temperature of the fluid (1300°C). The constant B serves as a proxy for activation energy, and this function also includes a term to describe the change of this constant with depth (or height above the plume source) in a manner similar to an activation volume. Equation (A6) was fit to various values of activation energy (E_a) from 0-523 kJ/mol (Table 2). As an aside, (A5) should not be thought of as the only law to describe the temperature dependence of viscosity; E_a is not really an energy per se, but is simply a constant to describe a temperature dependence. In fact, many materials, including most basaltic melts, display non-Arrhenian relationships between viscosity and temperature, and so we regard (A6) as being sufficiently accurate for the present analysis.

The boundary layer equations are nondimensionalized according to

$$(r,z)=\frac{(R,Z)}{h} \tag{A7}$$

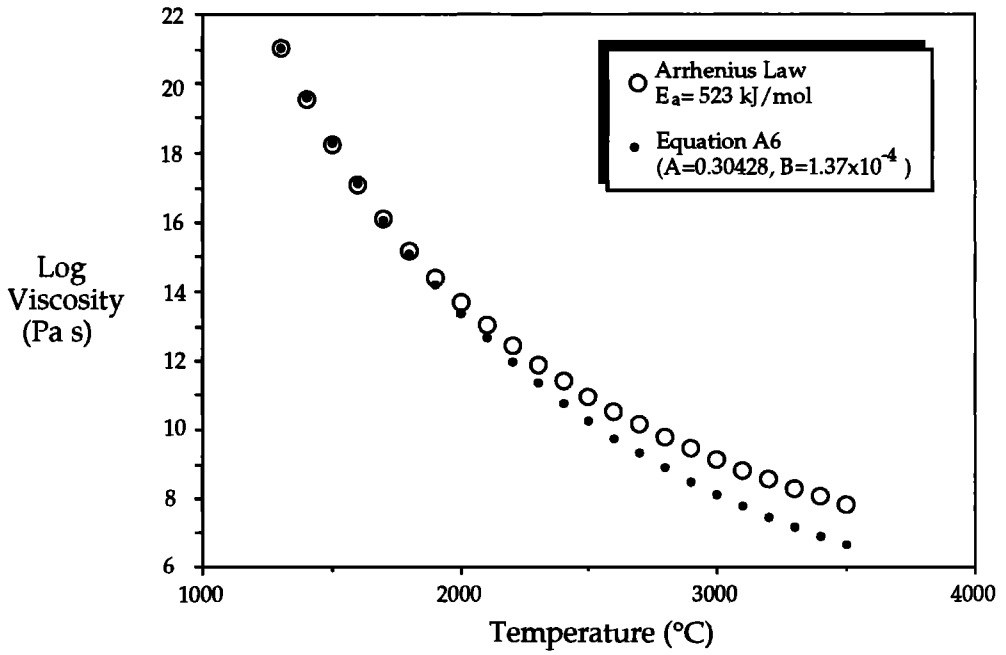

Figure A1. Plot of fluid viscosity as a function of temperature using Eq. (6) with A=0.30428, B=1.37×10^{-4} (filled circles), compared with Arrbenius law with an activation energy of 523 kL/mol (open circles).

$$(u,v)=(U,V)\frac{h}{\kappa} \tag{A8}$$

$$\theta=\frac{T-T_0}{\Delta T_{\text{base}}} \tag{A9}$$

where upper case letters represent dimensional, and lower case nondimensional, quantities. The base of the plume is taken to be at z=1, which means that the actual point source lies at a virtual origin some distance below the base of the plume. ΔT_{base} is the difference between the axial temperature at the base of the plume, and the ambient fluid temperature which is constant. Here θ is assumed to have a value of 1 on axis at the base of the plume (z=1), and decreases both with height above the base, and radially away from the axis. The length scale (h) is the distance from the base of the plume to the virtual origin (and the point source of heat). Substituting (A7)-(A9) into (A1)-(A4),(A6) gives the following dimensionless equations for momentum and energy:

$$\frac{\partial u}{\partial r}+\dot{\bar{F}}(-zB\Delta T_{\text{base}})\frac{\partial\theta}{\partial r}\frac{\partial u}{\partial r}+(\bar{F})^{-1/n}\left(\frac{\partial u}{\partial r}\right)^{\frac{n-1}{n}} z^{\frac{an-b}{n}} G\,\theta=0 \tag{A10}$$

$$u\frac{\partial\theta}{\partial z}+v\frac{\partial\theta}{\partial r}-\frac{1}{r}\frac{\partial}{\partial r}\left(r\frac{\partial\theta}{\partial r}\right)=0 \tag{A11}$$

where

$$\dot{\bar{F}}=^3exp\left[A-B\left(\frac{Z}{h}\right)\Delta T\right]\ ^2exp\left[A-B\left(\frac{Z}{h}\right)\Delta T\right] \bullet exp\left[A-B\left(\frac{Z}{h}\right)\Delta T\right] \tag{A12}$$

$$\bar{F}=^4\exp\left[A-B\left(\frac{Z}{h}\right)\Delta T\right] \tag{A13}$$

$$G=\frac{n\rho g\alpha_o\,\Delta T_{\text{base}}\,h^{\frac{n+2}{n}}}{(M\kappa)^{\frac{1}{n}}}\,C_1^{a}\,C_2^{-b/n}. \tag{A14}$$

The dimensionless parameter G is similar to that derived by *Yuen and Schubert* [1976] for the case of a boundary layer adjacent to a planar heat source. These equations are solved by the substitution of a stream function:

$$u=\frac{1}{r}\frac{\partial\Psi}{\partial r} \tag{A15a}$$

$$v=-\frac{1}{r}\frac{\partial\Psi}{\partial z} \tag{A15b}$$

and the similarity transformation is

$$\eta=r\,z^s \tag{A16}$$

$$\theta=z^{-1}\theta^*(\eta) \tag{A17}$$

$$\Psi=z\,f(\eta) \tag{A18}$$

where η is the independent similarity variable. After substitution of (A15)-(A18), the governing equation for conservation of momentum becomes

$$\eta^3f'''+(n-2)\eta^2f''+(2-n)\eta f'+\hat{\bar{F}}(-B\Delta T_{\text{base}}) \bullet(\eta^3f''-\eta^2f')\theta^{*'}+\bar{\bar{F}}^{-1/n}(\eta^2f''-\eta f')^{\frac{n-1}{n}} \bullet\left[r^4\right]\left[r^{-3}z\right]^{\frac{n-1}{n}} z^{\frac{an-b-n}{n}} G\,\theta^*=0 \tag{A19}$$

where

$$\hat{\bar{F}}=^3exp\left[A-B\Delta T_{\text{base}}\theta'\right]\ ^2exp\left[A-B\Delta T_{\text{base}}\theta\right] \bullet exp\left[A-B\Delta T_{\text{base}}\theta\right] \tag{A20}$$

$$\bar{\bar{F}}=^4\exp\left[A-B\Delta T_{\text{base}}\theta'\right]. \tag{A21}$$

In order for the solution to be valid, η must be the only independent variable, and thus the last term in (A19) must contain some power of η:

$$\left[r^4\right]\left[r^{-3}z\right]^{\frac{n-1}{n}} z^{\frac{an-b-n}{n}}=\left(rz^s\right)^x=\eta^x \tag{A22}$$

This condition is met when

$$s=\frac{(a-1)n-b-1}{n+3}\qquad x=\frac{n+3}{n} \tag{A23}$$

and (A19) becomes

$$\eta^3f'''+(n-2)\eta^2f''+(2-n)\eta f'+\hat{\bar{F}}(-B\Delta T_{\text{base}}) \bullet(\eta^3f''-\eta^2f')\theta^{*'}+\bar{\bar{F}}^{-1/n}(\eta^2f''-\eta f')^{\frac{n-1}{n}}\eta^{\frac{n+3}{n}} G\,\theta^*=0 \tag{A24}$$

After rearranging for η in (A24), the final forms of the momentum and energy equations are

$$f'''+(n-2)\frac{f''}{\eta}+(2-n)\frac{f'}{\eta^2}+(-B\Delta T_{\text{base}})\hat{\bar{F}}\left(f''-\frac{f'}{\eta}\right)\theta^{*'} +\bar{\bar{F}}^{-1/n}\left(f''-\frac{f'}{\eta}\right)^{\frac{n-1}{n}}\eta^{\frac{1}{n}} G\,\theta^*=0 \tag{A25}$$

$$\eta\theta^{*'}+f\,\theta^*=0. \tag{A26}$$

For the constant viscosity case (B=0) with a linear rheology (n=1), these equations reduce to the point-source equations of *Brand and Lahey* [1967] (assuming no inertial effects) and *Liu and Chase* [1991] (assuming zero compositional buoyancy).

The transformed momentum and energy equations are coupled ordinary differential equations in one variable and are integrated with a fourth order Runge-Kutta-Fehlberg algorithm using the shooting method. In this method of integration, the nonlinear properties of the governing equations are fully preserved, and it is computationally economical to use a fine grid, which is important for resolving the flow inside a plume in a fluid with variable viscosity. Equations (A25) and (A26) were solved subject to the boundary conditions:

$$\theta^*(0)=1 \quad \text{(A27)}$$

$$\theta^{*\prime}(0)=0 \quad \text{(A28)}$$

$$f(0)=0 \quad \text{(A29)}$$

$$f'(0)=0 \quad \text{(A30)}$$

$$f'(\infty)=0 \quad \text{(A31)}$$

$$\theta^*(\infty)=0 \quad \text{(A32)}$$

The flow is driven by the buoyancy of the plume as a result of an axial excess temperature at the base of the plume (ΔT_{base}). This temperature is specified (A27), and all other plume temperatures are normalized to this temperature. Equation (A30) indicates a stress free condition at the plume axis. Equation (A28) specifies zero temperature gradient at the plume axis; (A31) and (A32) indicate that the excess temperature and vertical velocity vanish far from the plume. An initial guess was made for f'', and the integration was iterated until the boundary conditions far from the plume were satisfied at η=5, which in the dimensional results discussed below corresponds to a distance of roughly 10,000-30,000 km from the plume axis.

The radial boundary of the plume is defined as the value of η where θ^* drops to 0.01; this is equivalent to the point at which the temperature excess drops to 1% of the axial value at a given height above the base of the plume. In this way, the entire heated mass of fluid within this radius at the base of the plume is defined as the plume source fluid, and any other ambient fluid which is heated by the plume, at any level above the base of the plume, is defined as entrained fluid. All of the plumes examined in this study entrain ambient fluid to some degree; entrainment is defined as the fraction of the total mass flux, at a given level, which is in excess of the mass flux at the base of the plume.

The results are dimensionalized by assuming the base of the plume starts at z=1. Thus, height above the base of the plume (Z^*) is related to the coordinate system through a virtual origin, where the virtual origin (Z=0) is located a distance h below the base of the plume:

$$z=Z/h=(Z^*+h)/h\,. \quad \text{(A33)}$$

Thus the point source is at (Z=0, z=0, Z^*=-h) and the base of the plume is at (Z=h, z=1, Z^*=0). Equation (A17) indicates that θ^* has a value of 1 at every point on the plume axis. Thus, combining (A9), (A17), and (A33), we see that the value of h is determined by the drop in temperature at the axis of the plume across a fixed depth D:

$$\frac{\Delta T_{base}}{\Delta T_{top}}=\frac{(D+h)}{h} \quad \text{(A34)}$$

where ΔT_{top} is the axial ΔT at the top of the plume. The vertical coordinate Z^* varies between 0 at the base of the plume and D at the top of the plume. Dimensional quantities are calculated from the non-dimensional results at any height Z^* from the following expressions:

$$\tau = M\left[C_2\left(\frac{Z^*+h}{h}\right)\right]^b\left[{}^4exp(A-B\Delta T_{base}\left(\frac{Z^*+h}{h}\right)^{-1}\theta^*\right] \cdot\left[\left(\frac{Z^*+h}{h}\right)^{3s+1}\left(\frac{f''}{\eta}-\frac{f'}{\eta^2}\right)\right]^{\frac{1}{n}} \quad \text{(A35)}$$

$$\mu=\tau\left[\left(\frac{\kappa}{h}\right)\left(\frac{Z^*+h}{h}\right)^{3s+1}\left(\frac{f''}{\eta}-\frac{f'}{\eta^2}\right)\right]^{-1} \quad \text{(A36)}$$

$$U=\left(\frac{\kappa}{h}\right)\left(\frac{Z^*+h}{h}\right)^{2s+1}\left(\frac{f'}{\eta}\right) \quad \text{(A37)}$$

$$V=\left(\frac{\kappa}{h}\right)\left(\frac{Z^*+h}{h}\right)^{s}\left(\frac{f}{\eta}+sf'\right) \quad \text{(A38)}$$

$$\Delta T=\left(\frac{Z^*+h}{h}\right)^{-1}\Delta T_{base}\theta \quad \text{(A39)}$$

$$R=\left(\frac{Z^*+h}{h}\right)^{-s}h\,\eta^* \quad \text{(A40)}$$

Since vertical velocity varies as z^s and the plume radius varies as z^{-s}, we can see that the plume volume flux (UR^2) is linear with height (z). In addition, since the axial ΔT varies as z^{-1}, plume heat flux (ΔTUR^2) is constant with height, and the plume conserves heat along its length. This is the expected result, since by definition, all the heat remains within the plume boundary. For each plume, a buoyancy flux (Q_B) was calculated:

$$Q_B = Q_m\ \alpha\ \overline{\Delta T} \quad \text{(A41)}$$

where Q_m is the plume mass flux and ΔT is the excess temperature integrated over the radius of the plume. Because of the trade-off between Q_m and ΔT with increasing radius away from the plume axis, Q_B is independent of the definition of the radius which defines the plume boundary. When examining plumes of different temperatures and rheologies, plumes with similar buoyancy fluxes were compared. All of the dimensional results were calculated from the nondimensional solutions assuming a layer depth D of 2700 km. A convenient notation for the drop in axial temperature of the plume across the depth of the fluid layer is the ratio ΔT_{base} / ΔT_{top}. For a given set of rheological and physical properties, each individual plume is determined by a value for ΔT_{top} and ΔT_{base},

and all other quantities (velocities, radii, buoyancy and mass fluxes, degree of entrainment) are results calculated from the numerical solutions of the governing equations. For this study, assumed values of ΔT_{top} [100°C 200°C 300°C 400°C] and the ratio $\Delta T_{base} / \Delta T_{top}$ [10 5.0 3.33 2.5 2.0 1.67 1.43 1.25 1.11 1.05] combine to produce 40 plumes for each set of physical and rheological properties. Results were calculated for two different power law exponents; n=1 for Newtonian fluids and n=3 for non-Newtonian fluids, each with (A6) fit to activation energies of 523, 423, 323, 223 and 0 kJ/mol at the top of each plume. Results for depth dependent thermal expansivity and viscosity were calculated independently in the n=1, 523 kJ/mol case, and comparisons were made for two different values for thermal diffusivity in this case as well, resulting in a total of 520 different plumes. Definitions and values for the various constants are given in Table 1.

Acknowledgments. We would like to thank all the participants of the W.M. Keck Geodynamics Seminar series at WHOI, the Caltech Plume Symposium, and Workshop on the Polynesian Plume Province for their interdisciplinary insights on this subject. We also thank D. Bercovici, B. Frazel, K. Helfrich, H. Dick, J. Blustzajn, N. Shimizu, G. Ravizza, M. Kurz, M. McNutt and F. Frey for their input during the long and tortuous history of this project. This work was supported by NSF grants EAR-8708372 (to S.R.H.), EAR-8916857 (to J.A.W.), a WHOI Mellon award, and NSF grant EAR-9315054 (to E.H.H. and J.A.W.).

References

Agee, C. B., and D. Walker. Mass balance and phase density constraints on the early differentiation of chondritic mantle, *Earth Planet. Sci. Lett., 90,* 144-156, 1988.

Albarede, F., How deep to common basaltic magmas form and differentiate?, *J. Geophys. Res., 97,* 10,997-11,009, 1992.

Allegre, C. J., Isotope geodynamics, *Earth Planet. Sci. Lett., 86,* 175-203, 1987.

Allegre, C. J., B. Hamelin, and B. Dupre, Statistical analysis of isotopic ratios in MORB: the mantle blob cluster model and the convective regime of the mantle, *Earth Planet. Sci. Lett., 71,* 71-84, 1984.

Allegre, C.J., B. Hamelin, A. Provost, and B. Dupre, Topology in isotopic multispace and origin of the mantle chemical heterogeneities, *Earth Planet. Sci. Lett., 81,* 319-337, 1987.

Boehler, R.,, Temperatures in the Earth's core from melting-point measurements of iron at high static pressures, *Nature, 363,* 534-536, 1993.

Brand, R. S., and F. J. Lahey, The heated laminar vertical jet, *J. Fluid Mech., 29,* 305-315, 1967.

Chase, C.G.,, Oceanic island lead: Two-stage histories and mantle evolution, *Earth Planet. Sci. Lett., 57,* 421-436, 1981.

Chen, C. Y., and F. A. Frey, Trace element and isotopic geochemistry of lavas from Haleakala Volcano, east Maui, Hawaii: Implications for the origin of Hawaiian basalts, *J. Geophys. Res., 90,* 8743-8768, 1985.

Chopelas, A., and R. Boehler, Thermal expansion measurements at very high pressure, systematics, and a case for a chemically homogeneous mantle, *Geophys. Res. Lett., 16,* 1347-1350, 1989.

Christensen, U.R., and D.A. Yuen, Layered convection induced by phase transitions, *J. Geophys. Res., 90,* 10,291-10,300, 1985.

Clague, D.A., R.T. Holcomb, J.M. Sinton, R.S. Detrick, and M.E. Torresan, Pliocene and Pleistocene alkalic flood basalts on the seafloor north of the Hawaiian Islands, *Earth Planet. Sci. Lett., 98,* 175-191, 1990.

Craig, H., and J. E., Lupton, Primordial neon, helium and hydrogen in oceanic basalts, *Earth Planet. Sci. Lett., 31,* 369-385, 1976.

Davies, G. F., Geophysical and isotopic constraints on mantle convection: An interim hypothesis, *J. Geophys. Res., 89,* 6017-6040, 1984.

Davies, G. F., Ocean bathymetry and mantle convection, 1, Large-scale flow towand hotspots, *J. Geophys. Res., 93,* 10,467-10,480, 1988.

Desonie, D. L., R. A. Duncan, and M. D. Kurz, Helium isotopic composition of isotopically diverse basalts from hotspot volcanic lineaments in French Polynesia (abstract), *EosTrans. AGU, 72 (44),* Fall Meeting suppl., 536, 1991.

Duncan, R. A., and I. McDougall, Linear volcanism in French Polynesia, *J. Volcanol. Geotherm. Res., 1,* 197-227, 1976.

Farley, K. A., J. Natland, and H. Craig, Binary mixing of enriched and undegassed mantle components in Samoan lavas, *Earth Planet. Sci. Lett., 111,* 183-197, 1992.

Frey, F.A., and J. M. Rhodes, Intershield geochemical differences among Hawaiian volcanoes: Implications for source compositions, melting process and magma ascent paths, *Philos. Trans. R. Soc. London A, 342,* 121-136, 1993.

Galer, S. J. G. and R. K. O'Nions, Residence time of thorium, uranium and lead in the mantle with implications for mantle convection, *Nature, 316,* 778-782, 1985.

Goetze, C., and D. L. Kohlstedt , Laboratory study of dislocation climb and diffusion in olivine, *J. Geophys. Res., 78,* 5961-5971, 1973.

Griffiths, R. W., Thermals in extremely viscous fluids, including the effects of temperature-dependent viscosity, *J. Fluid Mech., 166,* 115-138, 1986.

Griffiths, R. W., and I. H. Campbell, Stirring and structure in mantle starting plumes, *Earth Planet. Sci. Lett., 99,* 66-78, 1990.

Griffiths, R. W., and I. H. Campbell, On the dynamics of long-lived plume conduits in the convecting mantle, *Earth Planet. Sci. Lett., 103,* 214-227, 1991.

Hart, S. R., Heterogeneous mantle domains: Signatures, genesis and mixing chronologies, *Earth Planet. Sci. Lett., 90,* 273-296, 1988.

Hart, S. R., D. C. Gerlach, and W. M. White, A possible new Sr-Nd-Pb mantle array and consequences for mantle mixing, *Geochim. Cosmochim. Acta, 50,* 1551-1557, 1986.

Hart, S. R., E. H. Hauri, L. A. Oschmann, and J. A. Whitehead, Mantle plumes and entrainment: The isotopic evidence, *Science, 256,* 517-520, 1992.

Hauri, E. H., and S. R. Hart, Re-Os isotope systematics of HIMU and EMII oceanic island basalts from the south Pacific Ocean, *Earth Planet. Sci. Lett., 114,* 353-371, 1993.

Hofmann, A. W., and S. R. Hart, An assessment of local and regional isotopic equilibrium in the mantle, *Earth Planet. Sci. Lett., 38,* 44-62, 1978.

Hofmann, A. W., and W. M. White, The role of subducted oceanic crust in mantle evolution, *Yearbook Carnegie Inst. Washington, 79,* 477-483, 1980.

Ito, E., W. M. White, and C. Goepel, The O, Sr, Nd and Pb isotope geochemistry of MORB, *Chem. Geol., 62,* 157-176, 1987.

Kellogg, L.H., and G.J. Wasserburg, The role of plumes in mantle helium fluxes, *Earth Planet. Sci. Lett., 99,* 276-289, 1990.

Kennedy, A.K., S.-T. Kwon, F.A. Frey, and H.B. West, The isotopic composition of post-shield lavas from Mauna Kea volcano, Hawaii, *Earth Planet. Sci. Lett., 103,* 339-353, 1991.

Kohlstedt, D.L., C. Goetze, and W.B. Durham, Experimental deformation of single crystal olivine with application to flow in the mantle, in *Petrophysics: The Physics and Chemistry of Minerals and Rocks,* edited by S.K. Runcorn, pp. 67-78, John Wiley, New York, 1976.

Kurz, M. Mantle heterogeneity beneath oceanic islands: some inferences from isotopes, *Philos. Trans. R. Soc. London A, 342,* 91-103, 1993.

Kurz, M. D., W. J. Jenkins, S. R. Hart, and D. Clague, Helium isotopic variations in volcanic rocks from Loihi seamount and the island of Hawaii, *Earth Planet. Sci. Lett., 66,* 388-406, 1983.

Kurz, M.D., M.O. Garcia, F.A. Frey, and P.A. O'Brien, Temporal helium isotopic variations within Hawaiian volcanoes: Basalts from Mauna Loa and Haleakala, *Geochim. Cosmochim. Acta, 51,* 2905-2914, 1987.

Lipman, P.W., D.A. Clague, J.G. Moore, and R.T. Holcomb, South

Arch volcanic field-newly identified young lava flows on the sea floor south of the Hawaiian Ridge, *Geology, 17*, 611-614, 1989.

Liu, M., and C.G. Chase, Evolution of midplate hotspot swells-numerical solutions, *J. Geophys. Res., 94*, 5571-5584, 1989.

Liu, M., and C. G. Chase , Boundary-layer model of mantle plumes with thermal and chemical diffusion and buoyancy, *Geophys. J. Int., 104*, 433-440, 1991.

Loper, D.E., The dynamical structures of D" and deep plumes in a non-Newtonian mantle, *Phys. Earth Planet. Inter., 34*, 57-67, 1984.

Loper, D. E., and F. D. Stacey, The dynamical and thermal structure of deep mantle plumes, *Phys. Earth Planet. Inter., 33*, 304-317, 1983.

Lupton, J. E., and H. Craig, Excess 3He in oceanic basalts: Evidence for terrestrial primordial helium, *Earth Planet. Sci. Lett., 26*, 133-139, 1975.

Machetel, P., and P. Weber, Intermittent layered convection in a model mantle with an endothermic phase change at 670 km, *Nature, 350*, 55-57, 1991.

Marty, B., and P. Lussiez, Constraints on rare-gas partition coefficients from analysis of olivine-glass from a picritic mid-ocean ridge basalt, *Chem. Geol., 106*, 1-7, 1993.

McKenzie, D., and M. J. Bickle, The volume and composition of melt generated by extension of the lithosphere, *J. Petrol., 29*, 625-679, 1988.

McKenzie, D., and R. K. O'Nions, Mantle reservoirs and ocean island basalts, *Nature, 301*, 229-231, 1983.

Morgan, W. J., Plate motions and deep mantle convection, *Mem. Geol. Soc. Am., 132*, 7-22, 1972.

Nataf, H.-C., and J. VanDecar, Seismological detection of a mantle plume?, *Nature, 364*, 115-120, 1993.

Olson, P., and H. Singer, Creeping plumes, *J. Fluid Mech., 158*, 511-531, 1985.

Olson, P., D. A. Yuen, and D. Balsiger, Mixing of passive heterogeneities by mantle convection, *J. Geophys. Res., 89*, 425-436, 1984.

Osako, M., and E. Ito, Thermal diffusivity of $MgSiO_3$ perovskite, *Geophys. Res. Lett., 18*, 239-243, 1991.

Parsons, B., and J. G. Sclater, An analysis of the variation of ocean floor bathymetry and heat flow with age, *J. Geophys. Res., 82*, 803-827, 1977.

Peltier, W.R., and L.P. Solheim, Mantle phase transitions and layered chaotic convection, *Geophys. Res. Lett., 19*, 321-324, 1992.

Ribe, N., and U. Christensen, Three-dimensional modeling of plume-lithosphere interaction, *J. Geophys. Res., 99*, 669-682, 1994.

Richards, M. A., and R. W. Griffiths, Thermal entrainment by deflected mantle plumes, *Nature, 342*, 900-902, 1989.

Richter, F. M., and N. M. Ribe, On the importance of advection in determining the local isotopic composition of the mantle, *Earth Planet. Sci. Lett., 43*, 212-222, 1979.

Roden, M. F., F. A. Frey, and D. A. Clague, Geochemistry of tholeiitic and alkalic lavas from the Koolau Range, Oahu, Hawaii: Implications for Hawaiian volcanism, *Earth Planet. Sci. Lett., 69*, 141-158, 1984.

Schlichting, H., *Boundary Layer Theory*, McGraw-Hill, New York, 1968.

Sleep, N. H., Gradual entrainment of a chemical layer at the base of the mantle by overlying convection, *Geophys. J., 95*, 437-447, 1988.

Sleep, N. H., Hotspots and mantle plumes: some phenomenology, *J. Geophys. Res., 95*, 6715-6736, 1990.

Sleep, N. H., Time dependence of mantle plumes: Some simple theory, *J. Geophys. Res., 97*, 20,007-20,019, 1992.

Sleep, N.H., M.A. Richards, and B.H. Hager, Onset of mantle plumes in the presence of preexisting convection, *J. Geophys. Res., 93*, 7672-7689, 1988.

Sparks, D.W., and E.M. Parmentier, Melt extraction from the mantle beneath spreading centers, *Earth Planet. Sci. Lett., 105*, 368-377, 1991.

Spiegelman, M., and T. Elliot, Consequences of melt transport for uranium series disequilibrium in young lavas, *Earth Planet. Sci. Lett., 118*, 1-20, 1993.

Stacey, F. D., and D. E. Loper, The thermal boundary-layer interpretation of D" and its role as a plume source, *Phys. Earth Planet. Inter., 33*, 45-55, 1983.

Staudacher, T., and C. J. Allegre, Noble gases in glass samples from Tahiti: Teahitia, Rocard and Mehetia, *Earth Planet. Sci. Lett., 93*, 210-222, 1989.

Stevenson, D. J., Sources of D", *Eos Trans. AGU, 74 (43)*, Fall Meeting suppl., 415, 1993.

Stille, P., D.M. Unruh, and M. Tatsumoto, Pb, Sr, Nd and Hf isotopic constraints on the origin of Hawaiian basalts and evidence for a unique mantle source, *Geochim. Cosmochim. Acta, 50*, 2303-2319, 1986.

Tackley, P.J., D.J. Stevenson, G.A. Glatzmaier, and G. Schubert, Effects of an endothermic phase transition at 670 km depth in a spherical model of convection in the Earth's mantle, *Nature, 361*, 699-703, 1993.

Turcotte, D. L., and E. R. Oxburgh, Continental drift, *Phys. Today, 22*, 30-39, 1969.

Watson, S., Rare earth element inversions and percolation models for Hawaii, *J. Petrol., 34*, 763-783, 1993.

Watson, S., and D.McKenzie, Melt generation by mantle plumes: A study of Hawaiian volcanism, *J. Petrol., 32*, 501-537, 1991.

West, H.B., D.C. Gerlach, W.P. Leeman, and M.O. Garcia, Isotopic constraints on the origin of Hawaiian lavas from the Maui Volcanic Complex, Hawaii, *Nature, 330*, 216-220, 1987.

White, W.M., $^{238}U/^{204}Pb$ in MORB and open system evolution of the depleted mantle, *Earth Planet. Sci. Lett., 115*, 211-226, 1993.

White, W. M., and A. W. Hofmann, Sr and Nd isotope geochemistry of oceanic basalts and mantle evolution, *Nature, 296*, 821-825, 1982.

Whitehead, J. A., and D. S. Luther, Dynamics of laboratory diapir and plume models, *J. Geophys. Res., 80*, 705-716, 1975.

Wilson, J. T., A possible origin of the Hawaiian Islands, *Can. J. Phys., 41*, 863-870, 1963.

Woodhead, J. D., P. Greenwood, R. S. Harmon, and P. Stoffers, Oxygen isotope evidence for recycled crust in the source of EM-type ocean island basalts, *Nature, 362*, 809-813, 1993.

Wright, E., and W. M. White, The origin of Samoa: New evidence from Sr, Nd and Pb isotopes, *Earth Planet. Sci. Lett., 81*, 151-162, 1987.

Wysession, M. E., Lateral scales of heterogeneity at the base of the mantle, *EosTrans. AGU, 74 (43)*, Fall Meeting suppl., 415, 1993.

Young, C. J., and T. Lay, The core-mantle boundary, *Annu. Rev. Earth Planet. Sci., 15*, 25-46, 1987.

Yuen, D. A., and G. Schubert, Mantle plumes: A boundary layer approach for Newtonian and non-Newtonian temperature-dependent rheologies, *J. Geophys. Res., 81*, 2499-2510, 1976.

Zindler, A., and S. R. Hart, Chemical geodynamics, *Annu. Rev. Earth Planet. Sci., 14*, 493-571, 1986.

S. R. Hart and J. A. Whitehead, Department of Geology and Geophysics, Woods Hole Oceanographic Institution, Woods Hole, MA 02543.

E. H. Hauri, Department of Terrestrial Magnetism, Carnegie Institution of Washington, 5241 Broad Branch Road N.W., Washington, DC 20015. (email: hauri@dtm.ciw.edu)

(Received July 26, 1993; revised April 4, 1994; accepted May 13, 1994.)